EUROPEAN ORGANIZATION FOR NUCLEAR RESEARCH

CERN-EP/87-50
5 March 1987

# COMPOSITENESS AT LEP II

ALEPH: A. Blondel and E. Milotti
DELPHI: D. Bloch, K. Hamacher, L. Lyons and D. Treille*)
L3: H. Fesefeldt
OPAL: L. Levinson, P. Mättig and N. Wermes
Theory: U. Baur, D. Dominici, M. Lindner, P. Méry, M. Perrottet, F. Renard, D. Schildknecht, B. Schrempp*), F. Schrempp, K.H. Schwarzer and D. Zeppenfeld

Presented by D. Treille at the
LEP 200 ECFA Workshop
Aachen, 29 September–1 October 1986

---

*) Convener

# COMPOSITENESS AT LEP II

ALEPH: A. Blondel, E. Milotti
DELPHI: D. Bloch, K. Hamacher, L. Lyons, D. Treille
L3: H. Fesefeldt
OPAL: L. Levinson, P. Mättig, N. Wermes
Theory: U. Baur[*], D. Dominici[**], M. Lindner[***], P. Méry[×], M. Perrottet[×], F. Renard[××], D. Schildknecht[×××], B. Schrempp[+], F. Schrempp[+], K.H. Schwarzer[+], D. Zeppenfeld[++]
Presented by D. Treille
CERN, Geneva, Switzerland

## 1. INTRODUCTION

A number of important issues have stimulated new physics concepts beyond the Standard Model: the proliferation of quarks and leptons with their repetitive generation pattern, the large number of free parameters (masses, mixing angles, gauge couplings), fine tuning of the Higgs mass, and the ambitious project to consistently include gravity. Depending on priorities, the spectrum of new concepts reaches from grand unified, supergravity, and superstring theories, at one end, to compositeness, the subject of our working group, at the other end. A recent review on 'Beyond the Standard Model physics' is found in Ref. [1].

The purpose of this report is an investigation of the potential of LEP II to unravel possible substructure of leptons, quarks, and, perhaps, of the $W^{\pm}$ and Z vector bosons. First exploratory answers were given in Ref. [2], the report of a previous LEP II Working Group (for a recent review on LEP II physics, see also Ref. [3]). The present report goes beyond Ref. [2] in many respects. The main new aspects are

i) inclusion of initial-state polarization as an analysing tool;
ii) a thorough investigation of $e^+e^- \to W^+W^-$, more precisely of compositeness-motivated deviations from the Standard Model;
iii) an exploration of the potential of LEP II to either confirm or seriously corner the concept of 'nearby' compositeness.

More effort was also invested in realistic error analyses and background estimates.

In the following we shall distinguish two scenarios, that of 'conventional' and that of 'nearby' compositeness. In conventional compositeness the quarks and leptons (and possibly the Higgs boson) are assumed to be composite, whilst $W^{\pm}$ and Z remain genuine gauge bosons. For consistency, the compositeness scale, which is a measure of the inverse size of the composite quarks and leptons, will be

$$\Lambda_{\text{conv}} \geq 1\ \text{TeV}\ , \quad \text{possibly} \gg 1\ \text{TeV}\ . \tag{1}$$

The main expected signatures of conventional compositeness at LEP II are new contact interactions:

i) new four-fermion contact interactions [4, 2], most safely in $e^+e^- \to e^+e^-$,
ii) gauge-invariant contact interactions in $e^+e^- \to W^+W^-$, $e^+e^- \to \gamma\gamma$, and $e^+e^- \to 2$ gluons,

*) Max-Kade Fellow, Fermi Nat. Accel. Lab., Batavia, Ill., USA.
**) Ist. di Fisica teorica, Univ. Florence, Italy.
***) Inst. für Physik und Astrophysik, Max-Planck-Inst., Munich, Fed. Rep. Germany
×) CNRS, Luminy, Marseilles, France.
××) Dépt. de Physique mathématique, Univ. scient. et techn. du Languedoc, Montpellier, France.
×××) Fak. für Physik, Univ. Bielefeld, Fed. Rep. Germany.
+) Sektion Physik, Theoretische Physik, Univ. Munich, Fed. Rep. Germany.
++) Physics Dept., Univ. Wisconsin, Madison, Wisc., USA.

as explored by our Working Group in Section 2 (see also Refs. [5] and [6]). These contact interactions are to be understood as residual short-range interactions (due to some unknown confining gauge interactions among the quark-lepton constituents). Further composites, such as excited leptons and quarks or exotic fermions such as colour octet leptons, characteristic of schemes with coloured lepton constituents, are expected. They can only be observed directly at LEP II if they are exceptionally light compared to the naïve expectation of $m \approx O(\Lambda_{conv}) \gtrsim 1$ TeV. Otherwise, they manifest themselves through virtual exchanges, which essentially boils down again to the contact interactions (i) and (ii) at LEP II energies.

In the most radical version of compositeness, the so-called nearby compositeness, not only quarks and leptons, but also the $W^{\pm}$ and Z vector bosons are considered to be composite. This amounts to a reinterpretation of weak interactions as residual short-range interactions among composite particles (in much the same way as strong interactions are short-range, residual colour interactions among composite hadrons). The compositeness scale is set by the Fermi scale

$$\Lambda \approx O[(\sqrt{2}\, G_F)^{-1/2}] \approx O(250\,\text{GeV}) \ . \tag{2}$$

As this scale is close above the LEP II top energy, LEP II turns out, not surprisingly, to be a sensitive detector for many low-energy manifestations ($E \lesssim \Lambda$) of nearby compositeness. A possibly rich spectrum of further nearby composites, ground states as well as excited states, with lowest masses at most of the order of 1 TeV, is expected.

It is frequently advocated that their collective indirect effet manifests itself, as in conventional compositeness, in the form of new four-fermion contact interactions. This is correct to zeroth approximation only. Let us emphasize that valuable additional signals would be missed, such as i) mixing of new vector bosons with the photon (or gluons); ii) contact interactions already hidden in present low-energy data, such that $(8/\sqrt{2})G_F = g_W^2/m_W^2 + g_{new}^2/\Lambda^2$; iii) propagator effects of nearby new particles; iv) anomalous $WW\gamma$ and WWZ couplings; or v) possible exceptionally light particles, such as excited neutrinos (or electrons), or Goldstone-boson-type leptoquarks with very small couplings to fermion-antifermion pairs, etc. All these possible effects will be spelt out individually in this report.

In our selection of topics we intentionally remain as model-independent as possible. The discussion of anomalous $W^+W^-\gamma$ and $W^+W^-Z$ couplings in Section 4 starts from the most general (on-shell) expressions [7, 6, 8]. The new composite particles considered are: i) excited leptons, $e^*$ and $\nu^*$ (Section 3) (see also Refs. [9] and [6]); ii) an excited triplet $W^{\pm *}$ and $Z^*$, and a composite isoscalar vector partner Y of $W^{\pm}$ and Z, likely to appear in any model of nearby compositeness (Section 5) (see also Ref. [10]); iii) colour octet leptons, as characteristic signals of coloured lepton constituents (Section 7.1); and iv) light Goldstone boson leptoquarks, which could be pair-produced at LEP II (Section 7.2). An exception to the model independence is a discussion of the strongly coupled Standard Model in $e^+e^-$ reactions (see also Ref. [11]). Owing to its small number of free parameters it allows the prediction of correlated effects in different channels $e^+e^- \to e^+e^-$, $\mu^+\mu^-$, and $q\bar{q}$ (in particular, $b\bar{b}$); it has the interesting feature of implementing vector-boson leptoquarks and other exotic composites, with mass presumably well below 1 TeV, without the notorious conflict with the tight bounds on flavour-changing neutral currents.

The report concludes with a brief discussion of compositeness-motivated rare decay modes of the Z boson (see Ref. [9]).

Finally, in order to prevent misconceptions right from the start, let us point out two sources of ambiguities in extracting bounds for the compositeness scale $\Lambda$ from data. In general*), not $\Lambda$ but rather the ratio $g/\Lambda$ is measured, where g is the *unknown* effective coupling strength characteristic of the interaction of the composite particles involved. The ambiguity arises because in different schemes different conventions for g have become customary. The scale $\Lambda$, relevant for contact interactions in conventional compositeness, is determined under the assumption of

*) For composite isoscalar vector bosons which mix with the photon an absolute mass bound can be obtained.

strong coupling, $g^2/4\pi = 1$. In looking for electromagnetic form factors of composite leptons, the convention $g^2/4\pi = \alpha_{em}$ is commonly used. In nearby compositeness, for consistency, the measured weak coupling, $g_W \approx 0.65$, i.e. $g^2/4\pi \approx 0.03$, is appropriate. We shall stick to these conventions throughout this report. Let us emphasize that in comparing the extracted bounds on $\Lambda$ from different schemes, the appropriate 'rescaling' has to be performed; for example, two bounds

$$\Lambda \gtrsim 5\text{–}10 \text{ TeV} \tag{3}$$

from $e^+e^- \to f\bar{f}$ contact interactions and

$$\Lambda \text{ (or mass)} \gtrsim 1\text{–}2 \text{ TeV} \tag{4}$$

from nearby compositeness, are equivalent statements (the rescaling factor being $\sqrt{4\pi}/0.65 \approx 5.5$).

A second source of ambiguity is related to the issue of chiral symmetry. A consistent interpretation of quarks and leptons as composites requires a convincing mechanism to protect them from acquiring masses of the order of $\Lambda$. A favourite scheme is (approximate) chiral symmetry. In the absence of chiral symmetry, composite leptons contribute to $g - 2$ by means of the chirality-flipping operator

$$(g/\Lambda)\, \bar{\psi}_\ell(x)\, \sigma_{\mu\nu}\, \psi_\ell(x)\, F^{\mu\nu}(x) \tag{5}$$

in the Lagrangian. With this ansatz, data on $(g - 2)_\mu$ lead to the bound $\Lambda > 5 \times 10^6$ GeV, which would preclude any chance of detecting signals of compositeness at LEP II. The requirement of an (approximate) chiral symmetry reduces the coupling in Eq. (5) by $m_\mu/\Lambda$, leading to the cleanest bound from low-energy physics:

$$\Lambda > 720 \text{ GeV (90\% CL)} \; . \tag{6}$$

Issues in compositeness that are relevant for this report are reviewed in, for example, Refs. [12]–[14]. Most recent discussions of present bounds for compositeness are found in Refs. [14] and [15]. In summary, it can be stated [14] that present data do not exclude the option of nearby compositeness, leaving room for new composite particles with masses in the few hundred GeV range.

## 2. CONTACT INTERACTIONS

### 2.1 Four-lepton contact interactions [5]

In conventional compositeness, composite electrons necessarily give rise to new contact interactions [4] in Bhabha scattering, $e^+e^- \to e^+e^-$, and, if e and $\mu$ have constituents in common, also in $e^+e^- \to \mu^+\mu^-$. These can be detected through interference with the Standard Model amplitudes.

Our first objective was to reproduce the present limits obtained from PETRA and PEP [16], in order to check whether the criteria for statistical and systematic errors agree — which indeed they do.

Specific topics studied by our group (for details see Ref. [5]) are

i) a re-evaluation of the analysis of the preceding Workshop [2] under more realistic assumptions on systematic uncertainties and a comparison of the sensitivity of different observables;

ii) a closer study of the energy dependence of the visibility of contact interactions, in particular a confrontation of LEP II expectations with those obtained on top of the Z resonance, where a large luminosity is expected to be recorded;

iii) the introduction of initial-state ($e^{\pm}$) polarization; more precisely, the derivation of the corresponding $e^+e^- \to e^+e^-$, $\mu^+\mu^-$ cross-sections and an assessment of the importance of polarization for the detection of new contact interactions at LEP II.

Following Ref. [4], we concentrate on the most likely, i.e. helicity-conserving, contact interactions. For $e^+e^- \to e^+e^-$ the appropriate effective Lagrangian is

$$\mathcal{L} = \frac{g^2}{2\Lambda^2} \left[\eta_{LL}\, \bar{\psi}_L\gamma_\mu \psi_L\, \bar{\psi}_L\gamma^\mu \psi_L + \eta_{RR}\, \bar{\psi}_R\gamma_\mu \psi_R\, \bar{\psi}_R\gamma^\mu \psi_R + \eta_{RL}\, \bar{\psi}_R\gamma_\mu \psi_R\, \bar{\psi}_L\gamma^\mu \psi_L + \eta_{LR}\, \bar{\psi}_L\gamma_\mu \psi_L\, \bar{\psi}_R\gamma^\mu \psi_R\right] \qquad (7)$$

with unknown coefficients $\eta_{ij}$, normalized to $|\eta_{ij}| \leq 1$, and the convention $g^2/4\pi = 1$. (For $e^+e^- \to \mu^+\mu^-$, for consistency, $\mathcal{L}$ has to be defined without the overall factor 1/2.) The formulae for unpolarized [4] and polarized [5] cross-sections for $e^+e^- \to e^+e^-$, $\mu^+\mu^-$ are given in Appendix 1. Notice that the coefficient of the contact term in $e^+e^- \to e^+e^-$ is twice as large as in $e^+e^- \to \mu^+\mu^-$ owing to the additional presence of the t-channel exchange, a point which occasionally is treated incorrectly in the literature.

In Table 1 we list the various choices for the coefficients $\eta_{ij}$ which are customarily considered; furthermore, we include the new combinations [3]

$$\eta_{RR} = -\eta_{LL} = \pm 1\ , \quad \eta_{RL} = 0\ , \qquad (8)$$

which are 'orthogonal' to the $\gamma$ exchange term (in the sense of no interference). Correspondingly, they yield the poorest bounds on $\Lambda$ and serve in our analysis as a 'worst case study' (WCS). The probability for the unfavourable combination (8) is somehow reduced, however, since in $e^+e^- \to e^+e^-$ it cannot result from vector-boson exchange.

**Table 1**

Standard helicity configurations ($\eta_{LR} = \eta_{RL}$)

| | $\eta_{LL}$ | $\eta_{RR}$ | $\eta_{RL}$ |
|---|---|---|---|
| $LL_\pm$ | $\pm 1$ | 0 | 0 |
| $RR_\pm$ | 0 | $\pm 1$ | 0 |
| $VV_\pm$ | $\pm 1$ | $\pm 1$ | $\pm 1$ |
| $AA_\pm$ | $\pm 1$ | $\pm 1$ | $\mp 1$ |
| $WCS_\pm$ | $\pm 1$ | $\mp 1$ | 0 |

Let us first discuss the unpolarized case. Figure 1 shows the effect of contact interactions in the total cross-section and the forward-backward asymmetry $A_{FB}$ for $\Lambda = 5$ TeV. More information is obtained from the angular distributions, displayed in Fig. 2 for $\Lambda = 5$ TeV and $\sqrt{s} = 190$ GeV. This is confirmed by Fig. 3, which shows the sensitivity of $\sigma_{tot}$, $d\sigma/d\cos\theta$, and $A_{FB}$ for the AA and VV configurations at $\sqrt{s} = 190$ GeV, considering the different impact of the systematic errors on these observables. For the AA combination, with its strongly asymmetric angular distribution, $A_{FB}$ is as powerful as $d\sigma/d\cos\theta$.

In Fig. 4 we summarize the bounds on $\Lambda$, attainable at $\sqrt{s} = 190$ GeV, as a function of the luminosity for the various helicity combinations. A systematic error of 3% is included [5]. The LL and RR combinations lead to almost identical bounds; much more favourable are the combinations VV and AA. The WCS combinations (8) give poor bounds as expected.

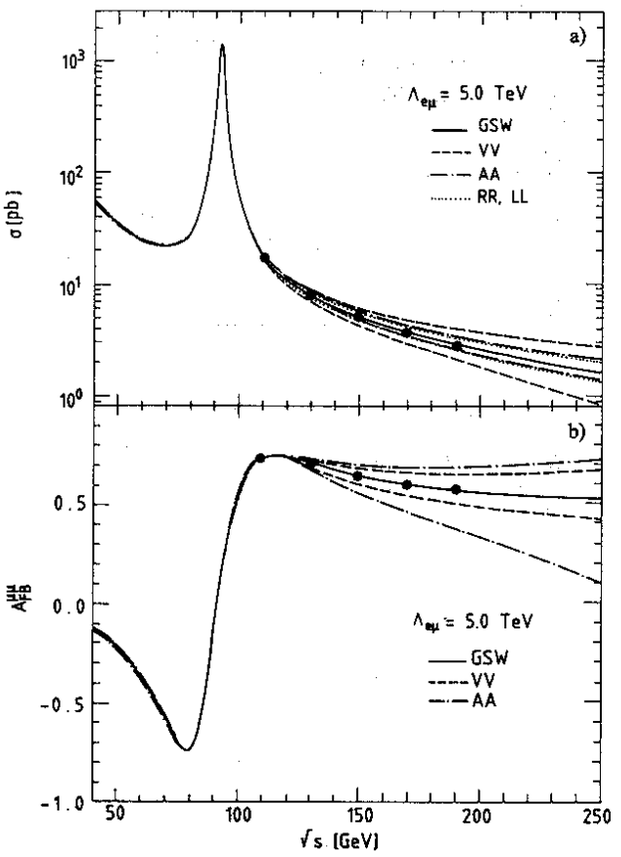


**Fig. 1** Effects of contact terms on a) $\sigma_{tot}$ and b) $A_{FB}$ for $e^+e^- \to \mu^+\mu^-$ as a function of $\sqrt{s}$. The curves above and below the Standard Model line (GSW) correspond to positive and negative interference, respectively. The 'data' points indicate the expected measurement accuracy for $\int L\,dt = 500\,pb^{-1}$ (Ref. [5]).

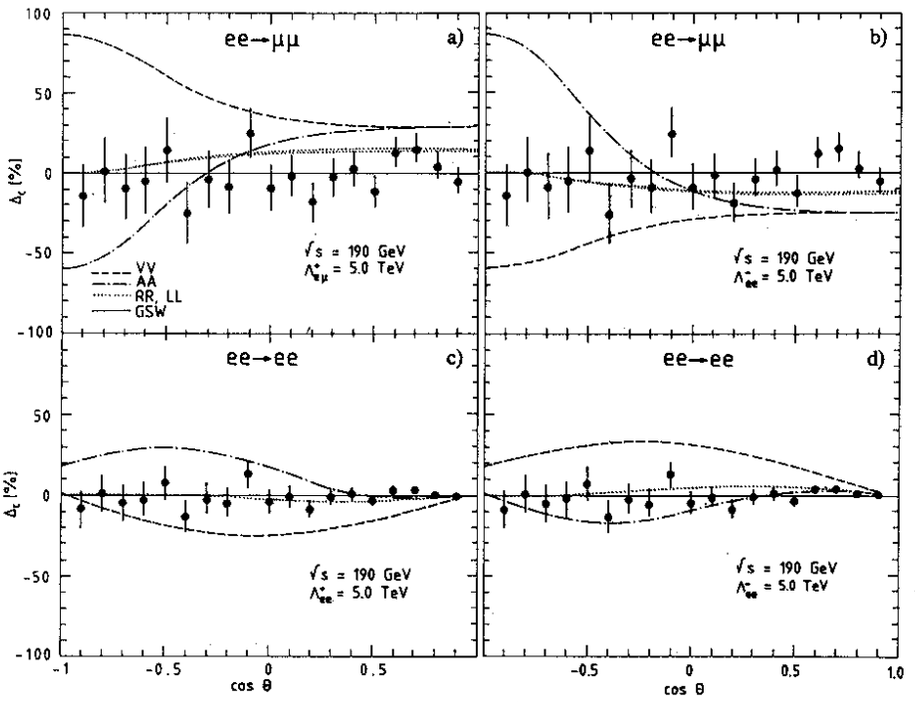


**Fig. 2** The effect of contact terms on $d\sigma/d\cos\theta$ for $e^+e^- \to \mu^+\mu^-$ [(a), (b)] and for $e^+e^- \to e^+e^-$ [(c), (d)], with positive [(a), (c)] and negative [(b), (d)] interference. The 'data' points represent a typical measurement at $\sqrt{s}$ = 190 GeV, for $\int L\,dt = 500\,pb^{-1}$; $\Delta_c$ is the relative deviation from the Standard Model cross-section (Ref. [5]).

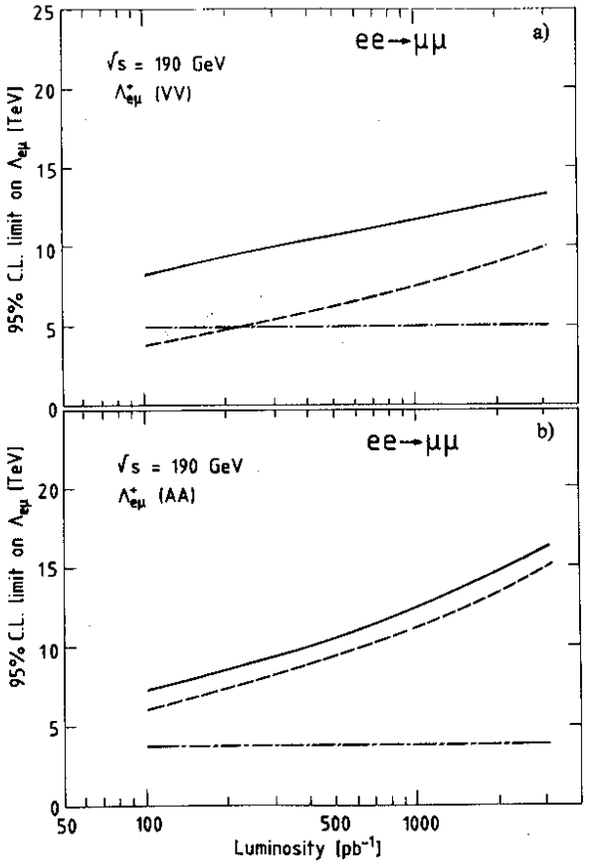


**Fig. 3** Comparison of the sensitivity of $d\sigma/d\cos\theta$ (solid line), $A_{FB}$ (dashed line), and $\sigma_{tot}$ (dash-dotted line) for contact terms with a) VV and b) AA helicity combinations. Here $A_{FB}$ has been assumed without systematic error (Ref. [5]).

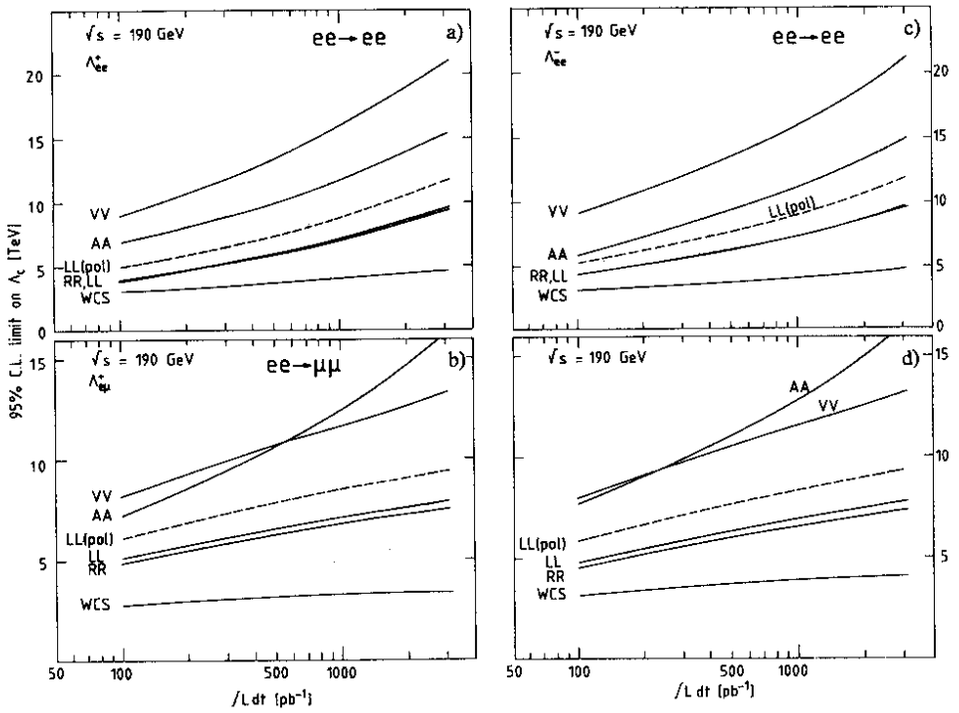


**Fig. 4** Lower bounds on the compositeness scale $\Lambda_c$ for $e^+e^- \to e^+e^-$ [(a), (c)] and for $e^+e^- \to \mu^+\mu^-$ [(b), (d)], as a function of the integrated luminosity at $\sqrt{s} = 190$ GeV. The various helicity combinations are explained in the text. The dashed line represents the case for LL, with a 50% longitudinally polarized $e^-$ beam, obtained from examining only $d\sigma/d\cos\theta$ (Ref. [5]).

Some analytical insight [3] into the dependence of the accessible value of $\Lambda$ on energy $\sqrt{s}$ and integrated luminosity $\int L\,dt$ may be obtained as follows. Disregarding systematic errors, the bound on $\Lambda$ can be obtained by equating the relative deviation

$$\left|[(d\sigma/d\cos\theta)_{\text{measured}}/(d\sigma/d\cos\theta)_{\text{Stand. Model}}] - 1\right| \underset{\substack{\uparrow \\ \text{assuming interference}}}{\propto} (s/\alpha\Lambda^2) , \quad (s \neq m_Z^2) , \tag{9}$$

with the corresponding statistical error of the measurement

$$1/\sqrt{N_{\text{evts}}} \propto 1/\sqrt{\int \alpha^2\, L\, dt/s} . \tag{10}$$

One deduces then the scaling law

$$\Lambda_{\text{bound}} \propto \sqrt[4]{\int L\, dt}\,\sqrt[4]{s} , \tag{11}$$

revealing i) that the bound on $\Lambda$ increases only fairly weakly with $\int L\, dt$ ('patience does not really pay'), and ii)

$$\Lambda_{\text{bound}} \propto \sqrt{s} \tag{12}$$

using the rule of thumb $\int L\, dt \propto s$.

These qualitative considerations are supported by exact calculations [3, 5] as shown in Fig. 5 for $\int L\, dt \approx 500\ \text{pb}^{-1}$ at $\sqrt{s} = 190$ GeV (still ignoring systematic errors). Figure 5 also demonstrates that the Z peak is particularly insensitive to contact interactions, since the imaginary electroweak amplitude does not interfere with the real contact interaction; maximal interference is only restored at the half-width positions on the tail of the Z.

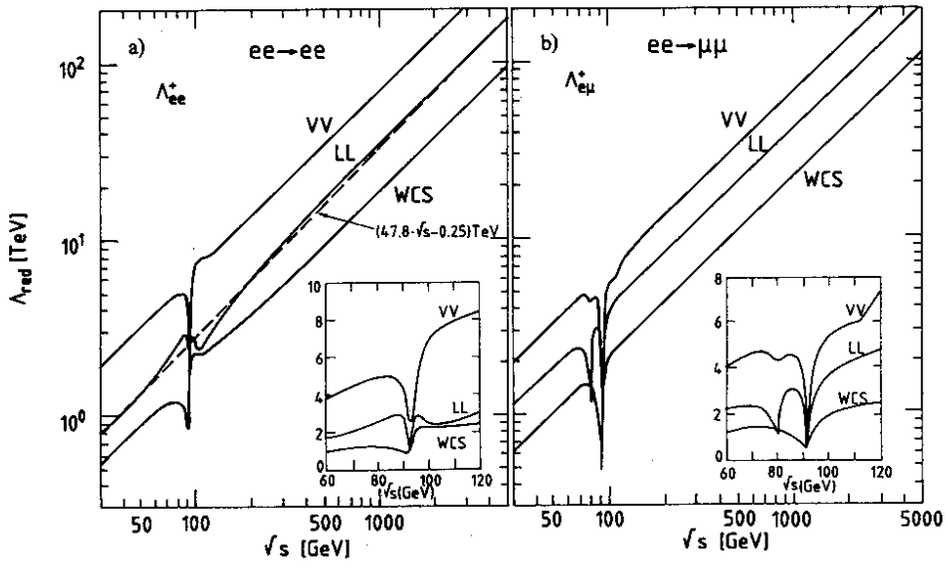


**Fig. 5** The 'reach' of $e^+e^-$ colliders, $\Lambda_{\text{red}} = \text{limit}\,(\Lambda_c)\cdot[[s/(190\ \text{GeV})^2]\cdot(500\ \text{pb}^{-1}/\int L\, dt)]^{1/4}$, as a function of $\sqrt{s}$, showing approximate scaling (dashed line). The most favourable (VV) and the most unfavourable (WCS) helicity combinations, as well as LL, are displayed. The inset shows the region around the Z. For the WCS, the exponent 1/4 in the definition of $\Lambda_{\text{red}}$ was replaced by 1/8 in order to obtain also approximate scaling. The reactions considered are a) $e^+e^- \to e^+e^-$ and b) $e^+e^- \to \mu^+\mu^-$ (Ref. [5]).

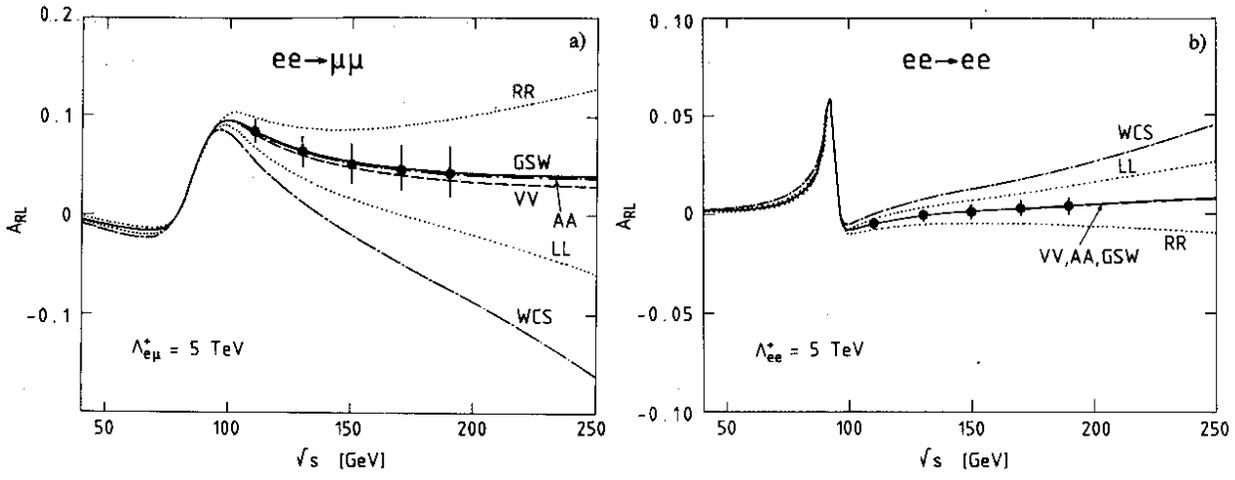


**Fig. 6** Effects of contact terms on $A_{LR}$ for a 50% longitudinally polarized $e^-$ beam. The 'data' points correspond to $\int L\,dt = 500\ pb^{-1}$, for the reactions a) $e^+e^- \to \mu^+\mu^-$ and b) $e^+e^- \to e^+e^-$ (Ref. [5]).

Figures 6 to 8 show the final results [5] for the bounds on Λ with 3% systematic error included. Clearly, without polarization (Fig. 6) the 'reach' for contact interactions at LEP II, as compared with PETRA or with expectations at the top of the Z resonance, is improved by roughly a factor of 4.

As may be expected, polarization hardly improves the bounds for the (in the unpolarized case) favourable helicity combinations VV and AA. It allows, however, to improve on the less favourable combinations LL and RR, depending on which beam is polarized, and considerably on the WCS combinations. This is demonstrated by the dashed line of Fig. 4, showing the bounds for LL with a 50% longitudinally polarized $e^-$ beam obtained from $d\sigma/d\cos\theta$.

The left–right asymmetry $A_{LR}$ is an even more powerful tool to exploit the fact that LL, RR, and WCS are sensitive to helicity interchanges (L → R). This is shown in Fig. 7 and included in Table 2.

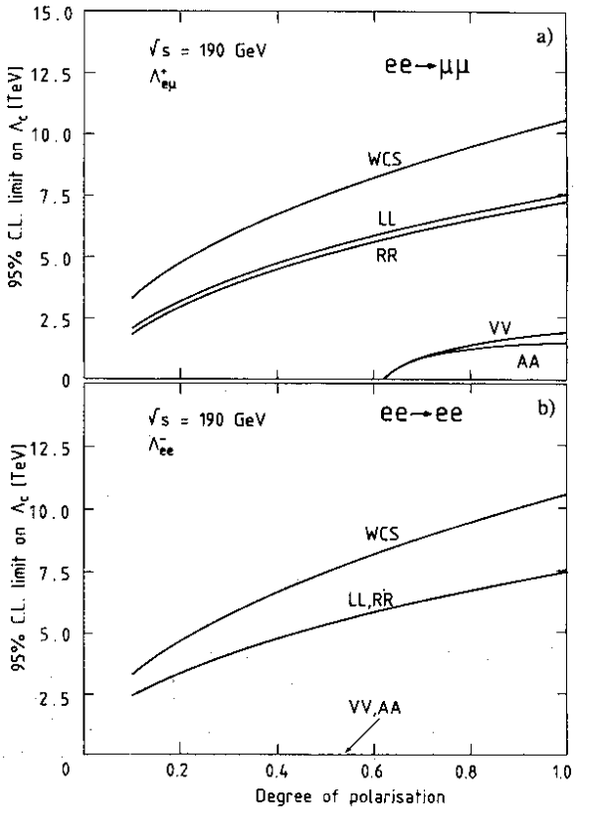


**Fig. 7** Lower bounds on $\Lambda_c$ obtained from $A_{LR}$ for a) $e^+e^- \to \mu^+\mu^-$ (positive interference) and b) $e^+e^- \to e^+e^-$ (negative interference). An error of 5% on the polarization measurement is assumed (Ref. [5]).

## Table 2

### Lower bounds on $\Lambda_c$

a) On $\Lambda_{ee}$ for $e^+e^- \to e^+e^-$

| $\sqrt{s}$ (GeV) | $\int L\,dt$ ($pb^{-1}$) | Polarization (%) $P_L^+$ | $P_L^-$ | $P_T$ | Interference | Obtained from | 95% CL limit (TeV) RR | LL | VV | AA | WCS |
|---|---|---|---|---|---|---|---|---|---|---|---|
| $m_Z - \Gamma_Z$ | 150 | unpolarized | | | pos. | $d\sigma/d\cos\theta$ | 3.2 | 3.6 | 6.4 | 4.3 | 1.0 |
| | | | | | neg. | | 3.2 | 3.6 | 6.4 | 4.4 | 2.0 |
| $m_Z$ | 150 | unpolarized | | | pos. | $d\sigma/d\cos\theta$ | 2.5 | 2.6 | 4.5 | 2.9 | 1.3 |
| | | | | | neg. | | 2.6 | 2.6 | 4.4 | 2.7 | 1.3 |
| $m_Z$ | 150 | – | – | +100 | pos. | $d^2\sigma/(d\cos\theta\,d\phi)$ | 3.6 | 3.6 | 4.8 | 3.6 | 4.8 |
| | | – | – | +50 | pos. | | 2.6 | 2.7 | 4.6 | 3.0 | 2.4 |
| $m_Z + \Gamma_Z$ | 150 | unpolarized | | | pos. | $d\sigma/d\cos\theta$ | 3.3 | 3.8 | 4.5 | 7.3 | 2.5 |
| | | | | | neg. | | 3.2 | 3.7 | 4.5 | 7.3 | 1.1 |
| 110 | 300 | unpolarized | | | pos. | $d\sigma/d\cos\theta$ | 3.4 | 3.3 | 9.2 | 9.1 | 2.6 |
| | | | | | neg. | | 3.5 | 3.4 | 9.3 | 8.9 | 2.1 |
| 190 | 500 | unpolarized | | | pos. | $d\sigma/d\cos\theta$ | 5.9 | 6.0 | 13.4 | 10.0 | 3.7 |
| | | | | | neg. | | 6.2 | 6.3 | 13.5 | 9.3 | 3.8 |
| 190 | 100 | unpolarized | | | pos. | $d\sigma/d\cos\theta$ | 3.9 | 4.0 | 9.0 | 6.9 | 3.1 |
| | | | | | neg. | | 4.3 | 4.4 | 9.2 | 5.8 | 3.1 |
| 190 | 500 | 0 | −100 | – | pos. | $d\sigma/d\cos\theta$ | 0.0 | 8.6 | 13.4 | 10.0 | 8.6 |
| | | 0 | −50 | – | pos. | | 4.0 | 7.4 | 13.4 | 10.0 | 5.9 |
| | | 0 | +50 | – | pos. | | 7.3 | 4.1 | 13.4 | 10.0 | 6.3 |
| | | 0 | −50 | – | neg. | | 4.5 | 7.6 | 13.5 | 9.3 | 6.5 |
| 190 | 250 + 250 | 0 | ±100 | – | pos. | $A_{LR}$ | 7.5 | 7.5 | 0.0 | 0.0 | 10.5 |
| | | 0 | ±50 | – | pos. | | 5.3 | 5.3 | 0.0 | 0.0 | 7.5 |
| 190 | 500 | – | – | +100 | pos. | $d^2\sigma/(d\cos\theta\,d\phi)$ | 5.9 | 6.0 | 13.5 | 10.3 | 3.7 |
| | | – | – | +50 | pos. | | 5.9 | 6.0 | 13.4 | 10.0 | 3.7 |

b) On $\Lambda_{e\mu}$ for $e^+e^- \to \mu^+\mu^-$

| $\sqrt{s}$ (GeV) | $\int L\,dt$ ($pb^{-1}$) | Polarization (%) $P_L^+$ | $P_L^-$ | $P_T$ | Interference | Obtained from | 95% CL limit (TeV) RR | LL | VV | AA | WCS |
|---|---|---|---|---|---|---|---|---|---|---|---|
| $m_Z - \Gamma_Z$ | 150 | unpolarized | | | pos. | $d\sigma/d\cos\theta$ | 2.5 | 3.1 | 5.3 | 2.6 | 2.0 |
| | | | | | neg. | | 2.5 | 3.1 | 5.3 | 2.6 | 1.4 |
| $m_Z$ | 150 | unpolarized | | | pos. | $d\sigma/d\cos\theta$ | 1.0 | 1.0 | 0.8 | 1.7 | 1.0 |
| | | | | | neg. | | 0.6 | 0.6 | 0.5 | 1.7 | 1.0 |
| $m_Z$ | 150 | – | – | +100 | pos. | $d^2\sigma/(d\cos\theta\,d\phi)$ | 1.2 | 1.2 | 1.9 | 1.9 | 1.0 |
| | | – | – | +50 | pos. | | 1.1 | 1.1 | 1.2 | 1.8 | 1.0 |
| $m_Z + \Gamma_Z$ | 150 | unpolarized | | | pos. | $d\sigma/d\cos\theta$ | 2.4 | 2.8 | 5.5 | 2.8 | 0.7 |
| | | | | | neg. | | 2.4 | 2.8 | 5.5 | 2.7 | 1.5 |
| 110 | 300 | unpolarized | | | pos. | $d\sigma/d\cos\theta$ | 3.3 | 3.6 | 5.3 | 5.7 | 1.5 |
| | | | | | neg. | | 3.1 | 3.5 | 5.8 | 5.3 | 2.0 |
| 190 | 500 | unpolarized | | | pos. | $d\sigma/d\cos\theta$ | 6.3 | 6.6 | 10.7 | 10.6 | 3.1 |
| | | | | | neg. | | 6.0 | 6.4 | 10.6 | 11.0 | 3.7 |
| 190 | 100 | unpolarized | | | pos. | $d\sigma/d\cos\theta$ | 4.9 | 5.1 | 8.2 | 7.2 | 2.8 |
| | | | | | neg. | | 4.5 | 4.8 | 8.0 | 7.7 | 3.2 |
| 190 | 500 | 0 | −100 | – | pos. | $d\sigma/d\cos\theta$ | 0.0 | 8.9 | 10.6 | 10.5 | 8.8 |
| | | 0 | −50 | – | pos. | | 4.4 | 7.9 | 10.7 | 10.6 | 6.3 |
| | | 0 | +50 | – | pos. | | 7.8 | 4.8 | 10.8 | 10.6 | 6.4 |
| | | 0 | −50 | – | neg. | | 4.1 | 7.7 | 10.5 | 11.0 | 6.7 |
| 190 | 250 + 250 | 0 | ±100 | – | pos. | $A_{LR}$ | 7.2 | 7.5 | 1.9 | 1.6 | 10.5 |
| | | 0 | ±50 | – | pos. | | 5.0 | 5.0 | 0.0 | 0.0 | 7.5 |
| 190 | 500 | – | – | +100 | pos. | $d^2\sigma/(d\cos\theta\,d\phi)$ | 6.5 | 6.9 | 10.7 | 10.6 | 3.8 |
| | | – | – | +50 | pos. | | 6.4 | 6.7 | 10.7 | 10.6 | 3.2 |

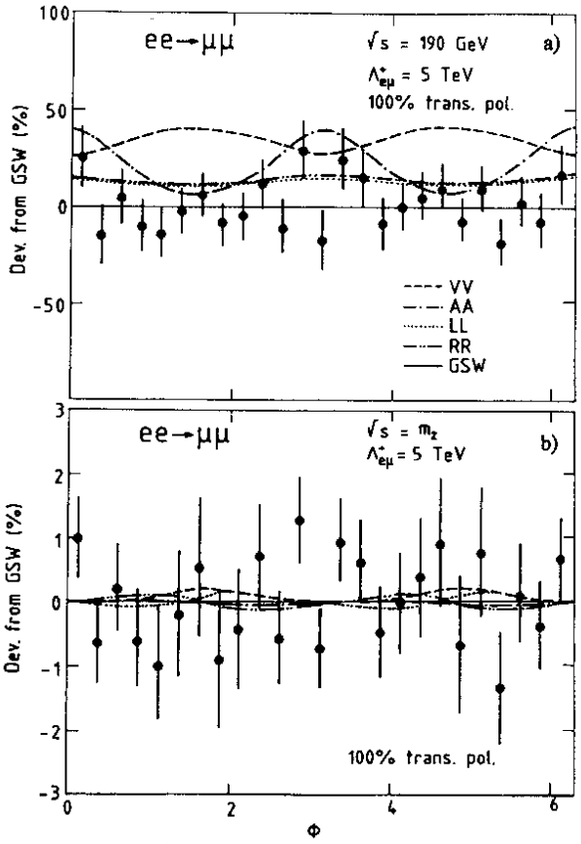


**Fig. 8** The effect of transverse polarization on $d\sigma/d\phi$ ($e^+e^- \to \mu^+\mu^-$) at a) $\sqrt{s} = 190$ GeV and b) $\sqrt{s} = m_Z$. The 'data' points indicate the measurement accuracy for a typical experiment with $\int L\,dt = 500\,pb^{-1}$ (Ref. [5]).

We conclude that by means of longitudinal polarization the sensitivity to the unfavoured configurations LL, RR, WCS is boosted to roughly the same level as the one for the combinations VV and AA, which are favoured for unpolarized beams. Transverse polarization introduces an azimuthal variation (Fig. 8). However, on top of the Z as well as at LEP II, this turns out to be a rather small effect, without noticeable improvement for the bounds on $\Lambda$.

Table 2 summarizes [5] the bounds on $\Lambda_c$ which can be *realistically* obtained at LEP II (implementing statistical and systematic errors); they range from 4 TeV to 13 TeV, depending on helicity combination and initial-state polarization.

### 2.2 Contact terms in $e^+e^- \to W^+W^-$

In Ref. [6] an exhaustive study of possible compositeness-motivated effects in $e^+e^- \to W^+W^-$ was performed, among them effects of $e^+e^-W^+W^-$ contact interactions. Two cases have to be distinguished. If the $W^\pm$ are gauge bosons (conventional compositeness), the contact interactions have to preserve local $SU(2)_L$ gauge invariance, and correspondingly only transverse components of $W^\pm$ are admitted. For composite $W^\pm$ also the longitudinal components may contribute to contact interactions.

#### 2.2.1 Gauge boson $W^\pm$

Most significant effects turn out to come from contact interactions of the form

$$\begin{aligned}&(g^2/2\cdot\Lambda^4)\bar{v}(k_2)\{(m_W^2 - t)(\not\epsilon_2\epsilon_1\cdot k_2 - \not\epsilon_1\epsilon_2\cdot k_1) + \\ &(m_W^2 - u)(\not\epsilon_1\epsilon_2\cdot k_2 - \not\epsilon_2\epsilon_1\cdot k_1) + (u - t)\not p_1\epsilon_1\cdot\epsilon_2 + \\ &2\cdot\not p_2(\epsilon_2\cdot k_2\epsilon_1\cdot k_1 - \epsilon_2\cdot k_1\epsilon_1\cdot k_2)\}(c - d\gamma^5)u(k_1)\end{aligned} \tag{13}$$

for $e^-(k_1) + e^+(k_2) \to W^-(\epsilon_1,p_1) + W^+(\epsilon_2,p_2)$. The coupling is normalized to $g^2(c^2 + d^2)/4\pi = 1$.

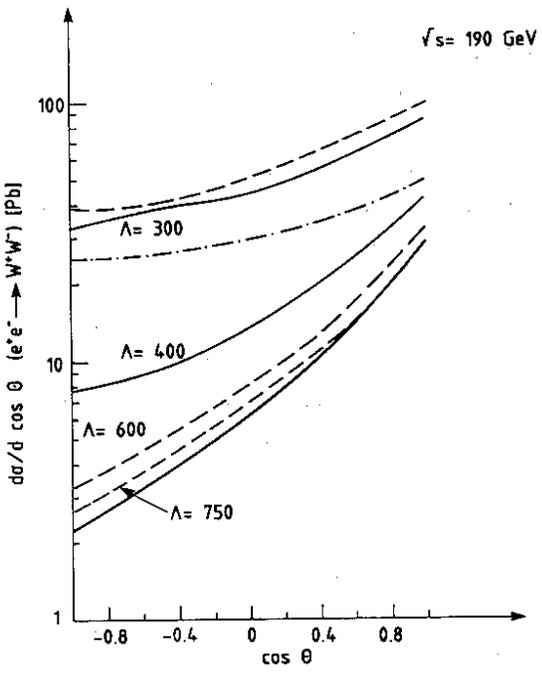


**Fig. 9** The $e^+e^- \to W^+W^-$ differential cross-section at $\sqrt{s}$ = 190 GeV obtained in the presence of contact terms (transverse amplitudes) $R_{TT}^{(2)}$, varying $\Lambda$ from 300 to 750 GeV. Full curves correspond to $R_{TT}^{(2)}$ (vector case). Dashed curves correspond to $R_{TT}^{(2)}$ (left-handed case) and dash-dotted curves to $R_{TT}^{(2)}$ (right-handed case).

Figure 9 shows the expected effect on the $e^+e^- \to W^+W^-$ differential cross-section for three representative helicity combinations: vector, left-handed, and right-handed. The contact term with right-handed coupling is most unfavourable, since it has no interference with the Standard Model $\nu$ exchange. In the most favourable case of a left-handed coupling, LEP II should be sensitive to values $\Lambda \lesssim 750$ GeV. This bound has to be compared with the much larger bound, of the order of 10 TeV, attainable from four-lepton contact interactions.

### 2.2.2 Composite $W^{\pm}$

Including longitudinal components of $W^{\pm}$ does not enhance the sensitivity to $e^+e^-W^+W^-$contact interactions at LEP II energies. However, for values of $\Lambda$ in the several hundred GeV range, contributions from longitudinal W's can be identified by their angular distributions, which deviate characteristically from the Standard Model prediction, as may be seen in Fig. 10.

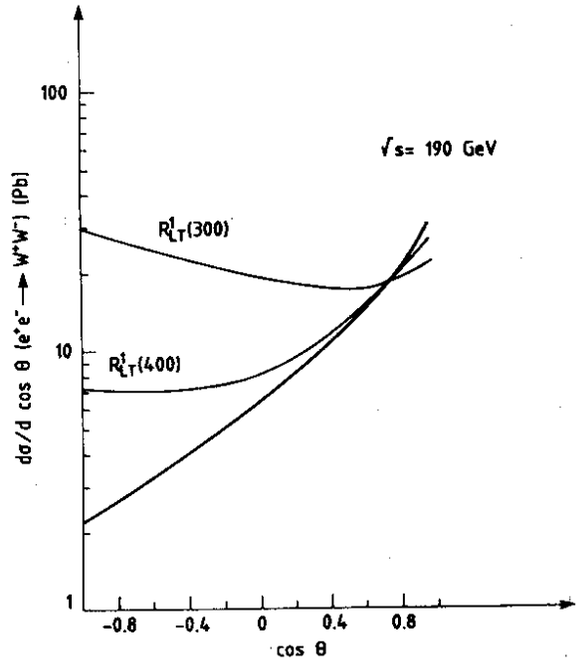


**Fig. 10** The same with both T and L components

## 3. EXCITED LEPTONS

Excited leptons are among the safest predictions of compositeness and therefore deserve particular attention. They may be expected to carry similar electroweak charges as leptons and to have (gauge-invariant) magnetic couplings to lepton-vector boson ($\gamma$,Z,$W^{\pm}$) pairs.

Possible manifestations of excited leptons at LEP II strongly depend on their mass values. Naïvely, one would expect masses of the order of the compositeness scale $\Lambda$. If for some reason excited leptons were exceptionally light, they can be pair-produced at LEP II in $e^+e^- \to \ell^*\bar{\ell}^*$ (see Fig. 11a). As was shown already [2, 17] a sensitivity up to masses close to the beam energy can be reached.

More realistically, one might hope to see them in single production, $e^+e^- \to \ell^{*\pm}\ell^{\mp}$, up to masses $M_{\ell^*} <$ 190 GeV. This is particularly feasible for excited electrons where the forward cross-section is strongly enhanced by the t-channel exchange graph (see Fig. 11b). Finally, for masses above 190 GeV, indirect manifestations become relevant: by virtual $e^*$ exchange in $e^+e^- \to \gamma\gamma$ (see Fig. 11c), and by $\nu^*$ exchange in $e^+e^- \to W^+W^-$ (see Fig. 11d).

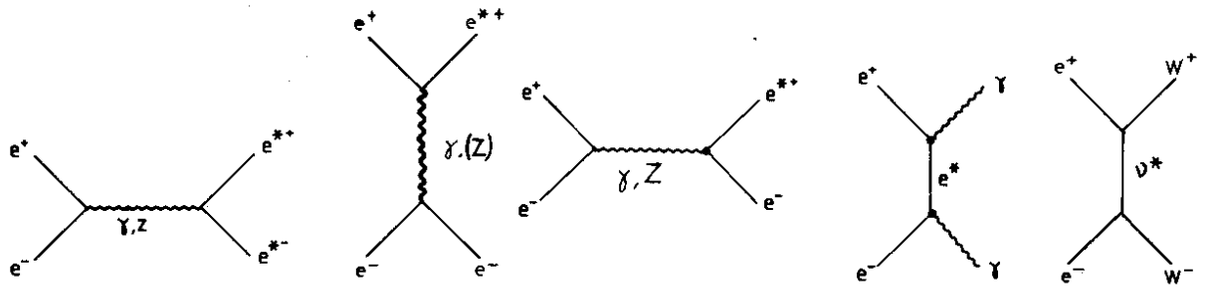


a) pair production b) single production c) $e^*$ exchange in $e^+e^- \to \gamma\gamma$ d) $\nu^*$ exchange in $ee \to W^+W^-$

**Fig. 11** The different diagrams involving excited leptons

Representative cross-sections for single $e^*$ production were already presented in Refs. [2] and [17]. Here we provide the necessary calculations of the Standard Model 'backgrounds', $e^+e^- \to e^+e^-\gamma$ for single $e^*$ production and $e^+e^- \to \gamma\gamma$ for $e^*$ exchange (see also Ref. [9]), and $e^+e^- \to W^+W^-$ for $\nu^*$ exchange (see also Ref. [6]). From this analysis, we obtain quantitative results for the sensitivity of LEP II to excited electrons and neutrinos. For comparison, the sensitivity to singly produced $e^*$ on top of the Z is also determined.

We have considered an integrated luminosity of 500 $pb^{-1}$ at LEP II and 100 $pb^{-1}$ at the top of the Z resonance.

### 3.1 Single $e^*$ search [9]

Following previous works [18, 17], we parametrize the gauge-invariant effective Lagrangian describing a magnetic-type transition of spin-½ excited electrons to electrons as follows:

$$\mathcal{L}_{\text{eff}} = \sum_{v=\gamma,Z} e(\lambda/m_{e^*})\,\bar{\psi}_{e^*}\,\sigma^{\mu\nu}(c_v - d_v\gamma_5)\psi_e\partial_\mu V_\nu + \text{h.c.} \qquad (14)$$

The coupling $\lambda$ is related to the compositeness scale $\Lambda$ defined in the context of strong coupling $g^2/4\pi = 1$ by

$$\frac{1}{\Lambda^2} \simeq \alpha[(\lambda/m_{e^*})^2]\,(|c_v|^2 + |d_v|^2)\ . \qquad (15)$$

We chose $|c_v|^2 = |d_v|^2 = 1$, in agreement with the absence of electric dipole moments for the electron and muon, and g − 2 measurements; this leaves free an overall normalization factor $\lambda$.

**Table 3**

Values of $\sigma$ (pb) for single $e^*$ production with $(\lambda/m_{e^*})^2 = 10^{-6}\,GeV^{-2}$

| | LEP I ($\sqrt{s}$ = 93 GeV) | | LEP II ($\sqrt{s}$ = 190 GeV) | |
|---|---|---|---|---|
| | $m_{e^*}$ (GeV) | | | |
| | 50 | 85 | 100 | 180 |
| $\sigma$ total | 11.9 | 3.7 | 5.9 | 3.2 |
| Fraction due to $Z^0 \to ee^*$ | 54% | 16% | | |
| $\sigma$ with $10° < \theta_{lab} < 170°$ | 7.3 | 1.3 | 0.98 | 0.76 |
| Fraction due to $Z^0 \to ee^*$ | 88% | 44% | | |
| $\sigma$ after cuts | 6.9 | 1.2 | 0.90 | 0.73 |

The $e^+e^- \to e^{*\pm}e^{\mp}$ differential cross-section, taking into account $\gamma$ and Z exchange, is detailed in Ref. [17]. Far from the Z mass $(d\sigma/dt)(e^+e^- \to e^{*\pm}e^{\mp})$ is dominated by $\gamma$ exchange in the t-channel, and excited electrons are mainly produced in the forward direction. At LEP I, on top of the Z, Z decay in $e^*e$ could make a significant contribution, as is shown in Table 3, where $(\lambda/m_{e^*})^2 = 10^{-6}\,GeV^{-2}$ was assumed.

For the decay, we expect $e^{*\pm} \to e^{\pm}\gamma$ to be dominant at LEP energies. The $e^*$ resonance is narrow, $\Gamma_{e^* \to e\gamma} \approx (\alpha/2)(\lambda/m_{e^*})^2 m_{e^*}^3$, and the angular dependence of the produced electron follows

$$\frac{d\Gamma}{d\cos\alpha_e} \approx 1 + \cos\alpha_e \qquad \text{for spin-}\tfrac{1}{2}\,e^*\ [17]\ , \tag{16}$$

where, in the $e^*$ rest frame, $\alpha_e$ is the angle of the $e^-$ with respect to the $e^-$ beam.

The main source of background in the search for singly produced $e^*$ comes from first-order radiative corrections to $e^+e^- \to e^+e^-$, where a hard photon is emitted at a large angle from the initial or final state. Two Monte Carlo programs have been used to describe the process $e^+e^- \to e^+e^-\gamma$. The first one [19a] takes into account all contributions involving $\gamma$ exchange only. The second one [19b] is based on $\gamma$ and Z exchange in the s-channel.

At LEP I energy, $\sqrt{s} = m_Z$, we have added the results from these two programs. Indeed, we have checked that, at Born term level, adding the corresponding diagrams reproduces the total cross-section, with a precision of 2%, in the whole angular range $0° < \theta_{lab} < 180°$.

At LEP II energies, we have used only the first program [19a] with $\gamma$-exchange contributions. As we want to detect all three tracks at large angles, we can neglect the effect from initial photon bremsstrahlung, leading to a return to the Z centre-of-mass energy. Neglecting the interference terms between $\gamma$ and Z exchange leads to an overestimation of the background at large angles:

| $e^\pm$ diffusion angle range: | 0–45° | 45–90° | 90–180° |
|---|---|---|---|
| $\dfrac{\sigma_{Born}\,(\gamma \text{ exchange only})}{\sigma^{tot}_{Born}\,(e^+e^- \to e^+e^-)}$: | 1–1.1 | 1.1–1.7 | 1.7–2.5 |

As $e^*$ are produced mainly at small angles at LEP II, this method gives a reasonable background estimate.

In order to minimize the background, it is necessary to detect each of the three tracks $e^+$, $e^-$, and $\gamma$ within the acceptance $10° < \theta_{lab} < 170°$. This choice of angular range will give a slightly better result than $2° < \theta_{lab} < 178°$ or $45° < \theta_{lab} < 135°$. We then require

i) $E_\gamma > 0.2E_{beam}$ and $E_{e\pm} > 0.05E_{beam}$, which should allow us to detect $e^*$ in the range $\sqrt{s}/4 \lesssim m_{e^*} < 0.95\sqrt{s}$ ;

ii) we remove Bhabha events with one almost collinear hard photon, setting $\theta_{\gamma e\pm} > 10°$ and $10° < \theta_{e^+e^-} < 170°$.

We are thus left with a background cross-section $\sigma(e^+e^- \to e^+e^-\gamma)$ of 51.9 pb at LEP I and 7.0 pb at LEP II. The same cuts keep more than 92% of the $e^*$ signal generated in the angular acceptance with a mass $m_{e^*} > \sqrt{s}/2$ (see Table 3).

The $e^\pm$-photon invariant mass spectrum of the background is given by Fig. 12. We used the luminosities quoted earlier. We have assumed a 90% efficiency for the detection of each track. The estimated mass resolution is rather conservative: $\sigma_m = 2$ GeV at LEP I, 4 GeV at LEP II. For each mass bin we can then compute the single $e^*$ cross-section corresponding to a deviation of $2\sigma$, reduced by systematics.

The result is shown in Fig. 13, where a 95% CL limit on $(\lambda/m_{e^*})^2$ is plotted as a function of $m_{e^*}$ at LEP energies, together with previous results from PETRA [20]. A bound as small as $(\lambda/m_{e^*})^2 < 10^{-7}$ GeV$^{-2}$ can be

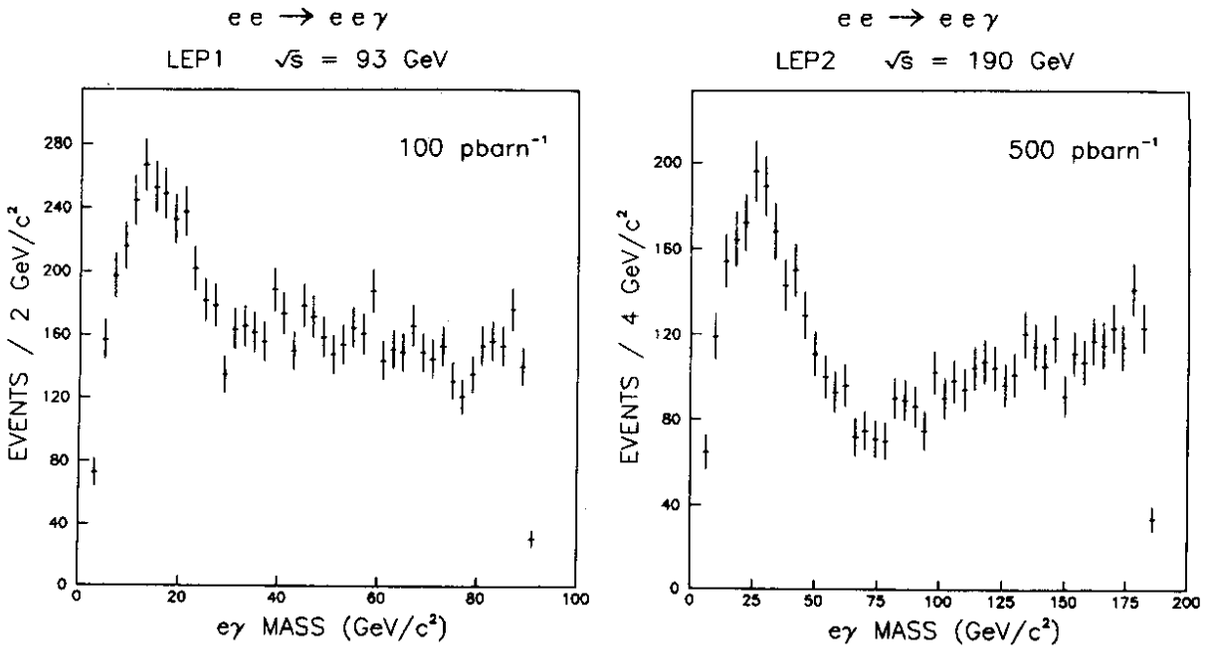


**Fig. 12** The $e\gamma$ invariant mass spectrum from Standard Model $e^+e^- \to e^+e^-\gamma$

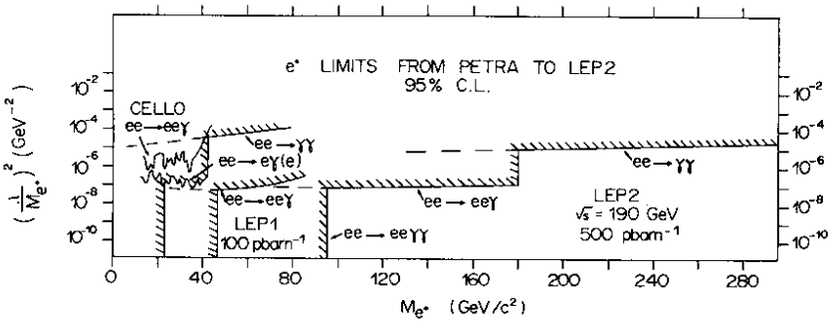


**Fig. 13** The limits on $e^*$ production resulting from different methods

achieved up to masses $m_{e^*}$ close to the centre-of-mass energy of LEP I and LEP II. At LEP II this bound may be translated, according to Eq. (15), into a sensitivity to couplings as small as

$$e\lambda = g \approx 0.02 \tag{17}$$

for $m_{e^*} = \Lambda$ close to the kinematical limit of 190 GeV.

Finally, let us comment on the possibility of spin-$^3/_2$ excited leptons [21]. The decay angular distribution (16) is replaced by $d\Gamma/d\cos\alpha_e \approx (1 + \cos\alpha_e)^3$, and the differential cross-section has to be changed appropriately. A rough check leads to a bound on $(\lambda/m_{e^*})^2$ at $\sqrt{s} = 190$ GeV which is about twice as high as the one for spin-$^1/_2$ excited electrons.

### 3.2 Virtual $e^*$ exchange [9]

The aim of this study is to look for a deviation in the angular dependence of the process $e^+e^- \to \gamma\gamma$ at LEP II, $\sqrt{s} = 190$ GeV. In the Standard Model this is a pure QED reaction, described at the level of the Born term by

$$\frac{d\sigma}{d\Omega}\ (e^+e^- \to \gamma\gamma) = (\alpha^2/s)(1 + \cos^2\theta)/(\epsilon^2 - \cos^2\theta)\ , \quad \epsilon \simeq 1 + 2m_e^2/s\ . \tag{18}$$

Radiative corrections of order $\alpha^3$ have been computed by means of a Monte Carlo program of Berends and Kleiss [22]. In order to select a pure sample of $\gamma\gamma$ events, we apply successively the following cuts which reduce the cross-section to the values given in the right-hand column:

| | $\sigma$ (pb) |
|---|---|
| - generated events with $\alpha^3$ radiative corrections | 112 |
| - at least two photons in acceptance $2° < \theta_{lab} < 178°$ | 30.6 |
| - if three photons generated, ask for $\theta_{\gamma\gamma} > 10°$ | 30.4 |
| - $E_{vis} > 0.8\sqrt{s}$ | 26.1 |
| - $\theta_{\gamma\gamma} > 170°$ between the two most energetic photons | 25.0 |
| - acoplanarity $< 10°$ between the two most energetic photons | 24.4 |

Assuming 90% efficiency for the detection of each photon and an integrated luminosity of 500 $pb^{-1}$ at LEP II, we are left with 9900 $\gamma\gamma$ QED events. Incidentally, such a large sample should be useful for decreasing the systematic uncertainty on the luminosity at LEP II, which we assumed to be 3%. The distribution $(d\sigma/d\Omega)_{exp}/(d\sigma/d\Omega)_{QED}$ is shown in Fig. 14, taking into account statistical fluctuations.

If a massive virtual excited electron is exchanged (Fig. 11c) the differential cross-section behaves according to [23]

$$(d\sigma/d\Omega)_{total}/(d\sigma/d\Omega_{QED}) = 1 \pm (s^2/2\Lambda_\pm^4)\sin^2\theta\, H(\cos^2\theta)\ , \tag{19}$$

where $H(\cos^2\theta) = a\,[a + (1 - \cos^2\theta)/(1 + \cos^2\theta)]/[(1 + a)^2 - \cos^2\theta]$, $a = 2m_{e^*}^2/s$, and $H(\cos^2\theta)$ tends to 1 as $m_{e^*} \gg \sqrt{s}$; $\Lambda_\pm$ is the QED cut-off parameter, related to the $e^*$ mass and the compositeness scale $\Lambda$ by

$$\frac{1}{\Lambda_\pm^4} = (\lambda/m_{e^*})^2\,(1/m_{e^*}^2) \approx (1/\Lambda^2)\,(1/\alpha m_{e^*}^2)\ . \tag{20}$$

In Fig. 14 virtual $e^*$ exchange is compared with the pure QED process. Significant deviations are expected at large angles $|\cos\theta_{lab}| \lesssim 0.5$. A $\chi^2$ calculation leads to a 95% CL limit on $\Lambda_\pm$, or on $m_{e^*}$ if $\lambda$ equals unity:

$$m_{e^*} > 260\ \text{GeV} \quad \text{if} \quad \lambda = 1\ . \tag{21}$$

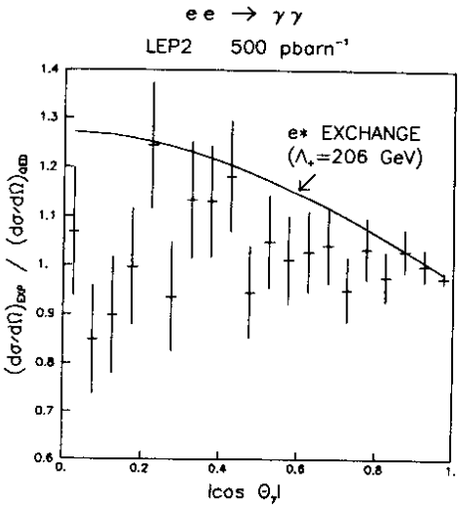


**Fig. 14** Deviation from QED in the angular dependence of the process $e^+e^- \to \gamma\gamma$. The error bars are statistical fluctuations from QED alone. The curve shows the effect of a heavy $e^*$ exchange.

This corresponds to a fairly powerful bound attainable at LEP II:

$$\Lambda \approx m_{e^*} > 3\ \text{TeV} \quad \text{if} \quad g^2 = 4\pi\ . \tag{22}$$

For an $e^*$ mass as large as a few TeV, at LEP II energies the $e^*$-exchange contribution to $e^+e^- \to \gamma\gamma$ 'shrinks' to a gauge-invariant contact term. The bound $\Lambda > 3$ TeV for this particular $e^+e^-\gamma\gamma$ contact interaction has to be compared with the one, $\Lambda > 4$–13 TeV, expected from four-lepton contact interactions.

### 3.3 $\nu^*$ exchange in $e^+e^- \to W^+W^-$

Virtual $\nu^*$-exchange in $e^+e^- \to W^+W^-$ at LEP II was discussed in Ref. [6]. The appropriate coupling is

$$\mathcal{L} = (g/2\Lambda)\, \bar{\psi}_{\nu^*}\, \sigma_{\mu\nu}\, W^{\mu\nu}(c - d\gamma_5)\psi_e + \text{h.c.}\ , \tag{23}$$

with c and d real (CP conservation). A natural choice is $\Lambda = m_{\nu^*}$. Within the convention of strong coupling, $g^2(c^2 + d^2) = 4\pi$, chosen in Ref. [6], LEP II is sensitive to $m_{\nu^*} \lesssim 700$ GeV. This is shown in Fig. 15. This mass bound has to be compared with the LEP II reach for virtual $e^*$ exchange, $m_{e^*} \lesssim 3$ TeV, derived in the preceding section.

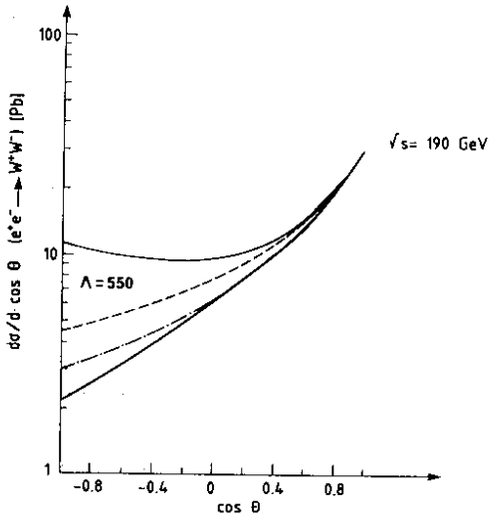


**Fig. 15** The effect of $\nu^*$ exchange in $e^+e^- \to W^+W^-$ at $\sqrt{s} = 190$ GeV and $m_{\nu^*} = \Lambda = 550$ GeV. The full curve refers to the vector or axial case. The dashed (dash-dotted) curve corresponds to the left-handed (right-handed) case.

## 4. ANOMALOUS WWZ and WWγ COUPLINGS AS REFLECTIONS OF COMPOSITENESS

An important objective of LEP II is a model-independent determination of the $ZW^+W^-$ and $\gamma W^+W^-$ couplings from $e^+e^- \to W^+W^-$. The aim is either to confirm their triple gauge-boson nature as predicted by the Standard Model or to pin down signals of new physics in general and, in the context of this report, of (nearby) compositeness in particular.

Three analyses have recently been performed:

i) The treatment of a DESY group [7] is completely general and involves all possible couplings, including CP-violating terms. The production of W's and their decay into $\ell\nu$ are treated; angular distributions and correlations of final leptons are presented. A systematic search is made to find the most sensitive distribution to a given anomalous coupling.

ii) The Marseilles–Montpellier analysis [6] is also quite general, although they limit themselves to CP-conserving terms.

iii) The approach of Ref. [8] is based on a conservative modification of the Standard Model and will be described separately at the end of the section.

### 4.1 The most general WWZ and WWγ couplings

The most general WWV vertex $\Gamma_V^{\alpha\beta\mu}$ is described [7] in terms of $2 \times 7$ independent form factors $f_i^V$

$$\begin{aligned}\Gamma_V^{\alpha\beta\mu}(q, \bar{q}, P) = \; & f_1^V (q - \bar{q})^\mu g^{\alpha\beta} - (f_2^V/m_W^2)(q - \bar{q})^\mu P^\alpha P^\beta + f_3^V (P^\alpha g^{\mu\beta} - P^\beta g^{\mu\alpha}) \\ & + i f_4^V (P^\alpha g^{\mu\beta} + P^\beta g^{\mu\alpha}) + i f_5^V \epsilon^{\mu\alpha\beta\varrho}(q - \bar{q})_\varrho \\ & - f_6^V \epsilon^{\mu\alpha\beta\varrho} P_\varrho - (f_7^V/m_W^2)(q - \bar{q})^\mu \epsilon^{\alpha\beta\varrho\sigma} P_\varrho (q - \bar{q})_\sigma \;, \end{aligned} \tag{24}$$

for $V = \gamma, Z$ and $g_{WW\gamma} = -e$, $g_{WWZ} = -e \cot\theta_w$. Whilst the form factors $f_i^V$ for $i = 1, 2, 3$ characterize couplings which are separately P and C conserving, for $i = 4, 6, 7$ they correspond to CP-violating ones, and for $i = 5$ to couplings separately violating P and C. For $i = 1, 2, 3$ they may be expressed in terms of the more familiar quantities $\kappa_V$ and $\lambda_V$ (for $g_1^Z = g_1^\gamma = 1$):

$$\begin{aligned} f_1^V &= 1 + (s/2m_W^2)\lambda_V \;, \\ f_2^V &= \lambda_V \;, \qquad\qquad V = \gamma, Z \;, \\ f_3^V &= 1 + \kappa_V + \lambda_V \;, \end{aligned} \tag{25}$$

which, in turn, are directly related to the W magnetic dipole and electric quadrupole moments

$$\begin{aligned} \mu_W &= e(1 + \kappa_\gamma + \lambda_\gamma)/2m_W \\ Q_W &= -e(\kappa_\gamma - \lambda_\gamma)/m_W^2 \;. \end{aligned} \tag{26}$$

In the Standard Model all the form factors $f_i^V$ vanish at tree level except for $f_1^V = 1$ or $\lambda_V = 0$, and $f_3^V = 2$ or $\kappa_V = 1$. Once the Standard Model constraints have been relaxed, there is a large number of free parameters to be tested for.

### 4.2 The LEP II sample of W pairs

In order to extract the boson couplings, the sample to be used has been chosen as follows [24]:

- integrated luminosity 500 $pb^{-1}$,
- $\sqrt{s} = 190$ GeV,

- $m_W$ = 80.3 GeV, $\sin^2\theta_w$ = 0.229, $m_t$ = 40 GeV,
- $\sigma_{tot}$ = 14.3 pb,
- one W goes into $\ell\nu$, with $\ell$ = e,$\mu$ well identified.

After selection, we thus get $\approx$ 1600 useful identified pairs. The systematic errors are

$$2\% \text{ from selection, } 3\% \text{ from luminosity .} \tag{27}$$

The background is negligible. The expected angular resolution on W (50 to 200 mrad) has not much effect on the present study.

Note that the authors of Ref. [7] have in fact considered a sample of 4000 useful W pairs.

### 4.3 Variation of a single coupling

The straightforward way to discuss the visibility of anomalous couplings is to vary one of them, keeping the others at the Standard Model value.

A first result of Ref. [7] illustrated by Fig. 16 is that the CP-violating terms are only marginally observable. As concerns CP-conserving terms, Fig. 17 (from Ref. [7]) shows that anomalies are best observable in the W differential cross-section: a 10% deviation from the standard value can be detected. A similar conclusion is reached by Ref. [6], as shown in Fig. 18.

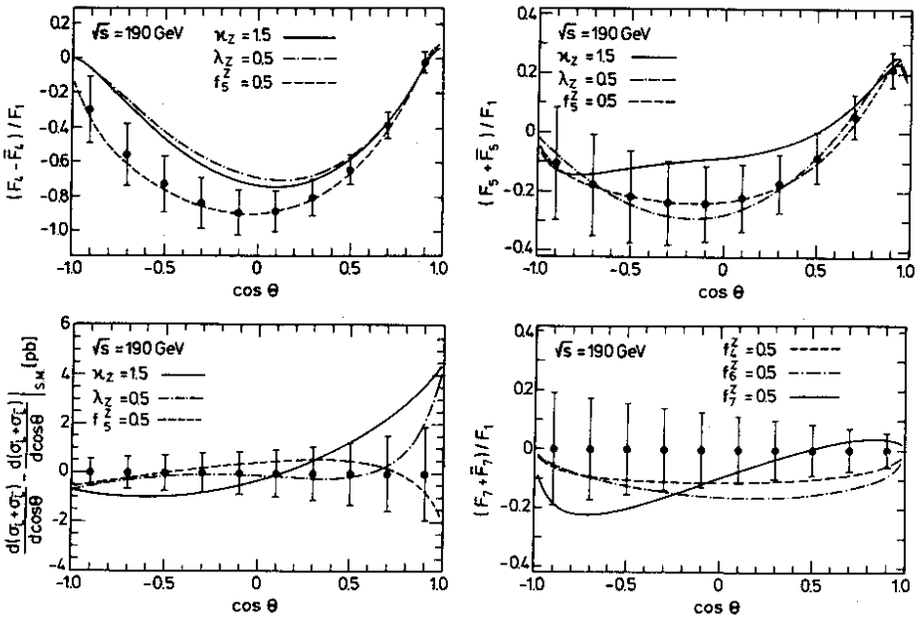


**Fig. 16** Various polarized W cross-sections, exhibiting different sensitivity to anomalous VWW couplings, compared with the statistical errors from 4000 decaying W's (from Ref. [7]). Couplings $f^Z_{4,6,7}$ are CP-violating.

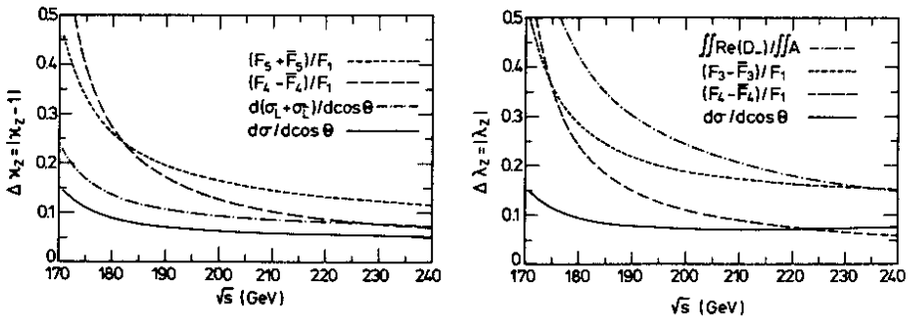


**Fig. 17** Minimum deviations of $\kappa_Z$ and $\lambda_Z$ from their Standard Model values to produce a $1\sigma$ effect in the four most sensitive angular distributions, displayed versus $\sqrt{s}$ (notations of Ref. [7]).

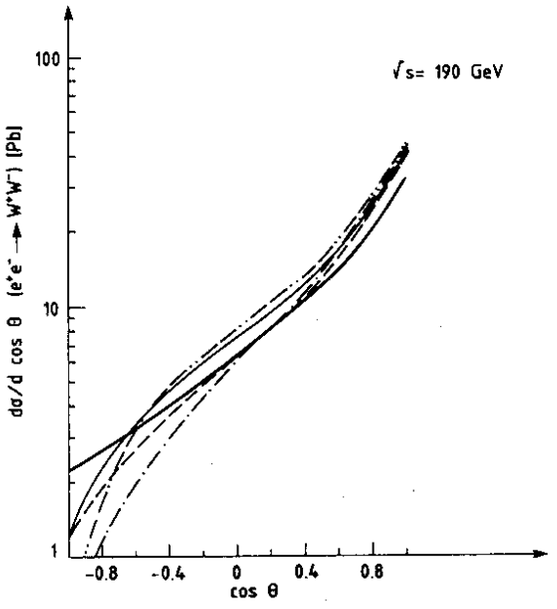


**Fig. 18** Angular distribution of $e^+e^- \to W^+W^-$ at $\sqrt{s} = 190$ GeV including anomalous W moments $\varkappa$ and $\lambda$. Full curve: $\lambda_Z = 1$; dashed curve: $\varkappa_Z = 2$; dash-dotted-dotted curve: $\lambda_\gamma = \lambda_Z = 1$; dash-dotted curve: $\varkappa_\gamma = \varkappa_Z = 2$.

Figure 17 also shows that increasing the energy does not greatly improve the sensitivity to anomalous couplings.

### 4.4 Correlated variations of the couplings [3, 25]

The situation becomes considerably worse, however, if multidimensional regions in parameter space are considered. The banana-shaped regions [3] in the $\varkappa_Z$-$\varkappa_\gamma$ and $\lambda_Z$-$\lambda_\gamma$ planes, computed and displayed in Fig. 19a, correspond to less than $1\sigma$ deviation from the Standard Model prediction of $d\sigma/d\cos\theta$! Figure 19b illustrates the strikingly different sensitivity in $d\sigma/d\cos\theta$, depending on the *correlation* of the parameters $\varkappa_\gamma$ and $\varkappa_Z$. Note that curve 3 corresponds to values $(\varkappa_Z - 1, \varkappa_\gamma - 1)$ close to the right-hand tip of the respective 'banana' of Fig. 19a. In curves 1 and 2, instead, *one* of the $\varkappa$'s takes its Standard Model value. The 'banana' effect is easily understood [3]. The sensitivity to anomalous couplings is largely due to their *interference* with the dominant neutrino-exchange graph, which, in turn, only contributes to the amplitudes with *left*-handed incoming electrons. The dashed lines along the $\varkappa$ and $\lambda$ 'bananas' in Fig. 19a correspond to linear combinations of anomalous $\gamma$ and Z couplings, such that at $\sqrt{s} = 190$ GeV the anomaly in the left-handed amplitudes (and thus the interference) exactly cancels, i.e. $\varkappa_L = 1$ and $\lambda_L = 0$. This implies that anomalous effects from possible new physics, contributing mainly to the *isoscalar* W form factors (such as heavy, isoscalar vector bosons), will be hard to detect experimentally.

In order to solve this ambiguity and therefore to distinguish $WW\gamma$ from WWZ form factors, a separate measurement of the right- and left-handed amplitudes $\mathfrak{M}_R$ and $\mathfrak{M}_L$ is required. This can be achieved to a certain extent by means of initial beam polarization [25].

For the general case of arbitrary longitudinal polarization $P_L^\pm$ and transverse polarization $P_T^\pm$ of the $e^\pm$ beams, the differential cross-section is given by

$$d\sigma \approx (1 - P_L^-)(1 + P_L^+)\,|\mathfrak{M}_L|^2 + (1 + P_L^-)(1 - P_L^+)\,|\mathfrak{M}_R^2| + 2P_T^- P_T^+ [\mathrm{Re}\,(\mathfrak{M}_L \mathfrak{M}_R^*)\cos 2\phi + \mathrm{Im}\,(\mathfrak{M}_L \mathfrak{M}_R^*)\sin 2\phi] \quad . \tag{28}$$

Here, summation over final-state helicities is implied and the azimuthal angle dependence is shown explicitly.

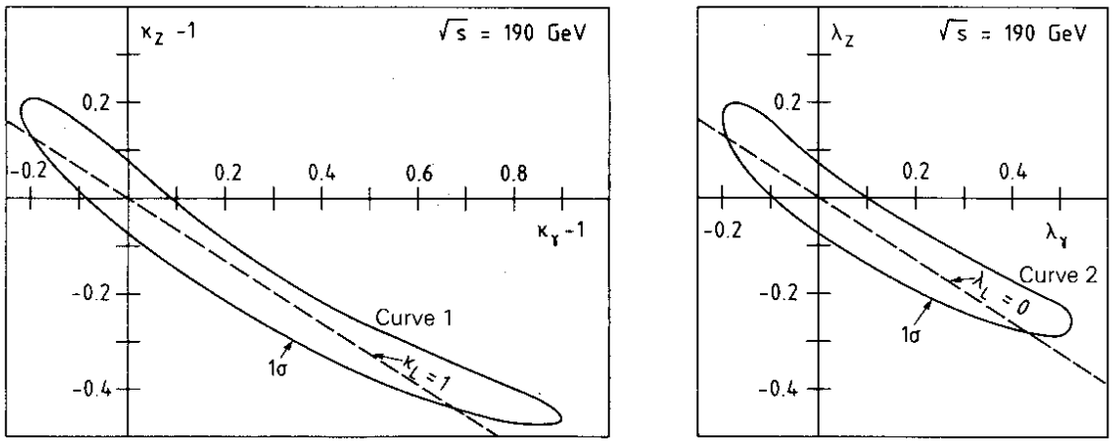


a) Regions in the $\kappa_Z$–$\kappa_\gamma$ (interior of curve 1) and $\lambda_Z$–$\lambda_\gamma$ (interior of curve 2) planes corresponding to less than $1\sigma$ deviation from the Standard Model prediction for $d\sigma/d\cos\theta$.

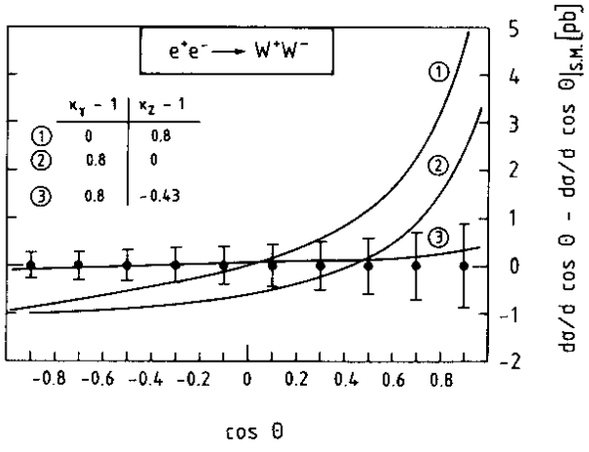


b) Sensitivity in $d\sigma/d\cos\theta$ for various correlations of anomalous couplings $\kappa_\gamma$ and $\kappa_Z$.

**Fig. 19**

For the Standard Model values of the form factors $f^\gamma$ and $f^Z$, one finds $|\mathfrak{M}_R|^2/|\mathfrak{M}_L|^2 \approx 10^{-2}$ over a large range of $e^+e^-$ centre-of-mass energies. Thus, without beam polarization, only about 80 W pairs can be produced from right-handed electrons with an integrated luminosity of 500 $pb^{-1}$ at $\sqrt{s}$ = 190 GeV. Since in practice longitudinal polarization — if it can be achieved at all — will not be perfect, these pairs will always be hidden in a background of a few thousand W pairs originating from the scattering of left-handed electrons. Owing to the limited statistics, $|\mathfrak{M}_R|^2$ can hence only be determined within a factor of 2–3, and a variation of $\mathfrak{M}_R$ due to anomalous couplings will thus be difficult to observe.

Beam polarization can be used in two different ways to increase the sensitivity to the right-handed combination $f_R$ of $\gamma$ and Z form factors. With longitudinal polarization, the 'signal' from $|\mathfrak{M}_R|^2$ can be increased, depressing the 'background' from $|\mathfrak{M}_L|^2$ simultaneously, or one can use transverse polarization to make $\mathfrak{M}_R$ interfere with the much larger $\mathfrak{M}_L$, which again enhances the signal. These two options have been studied in some detail [25]; the results are shown in Figs. 20a and 20b, showing the significance of deviations of $\kappa_\gamma$ and $\kappa_Z$ from their Standard Model values under conditions specified in the caption.

One conclusion is that substantial degrees of polarization $P_T$, $P_L$ are needed in order to improve significantly the detection capabilities of LEP II experiments for anomalous W-couplings. This is obvious for transverse polarization where the size of the effect (the $2\phi$ modulation) is proportional to $P_T^2$. With $P_T$ = 50%, for example,

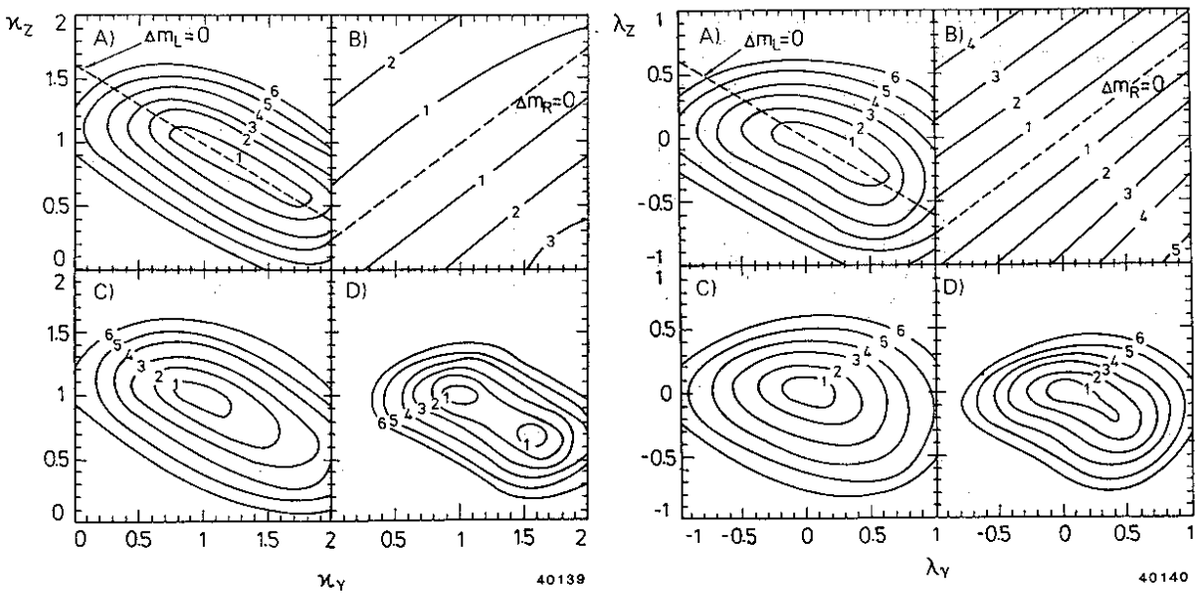


**Fig. 20** Significance of deviations of $\kappa_\gamma$ and $\kappa_Z$ (a) and of $\lambda_\gamma$ and $\lambda_Z$ (b) from their Standard Model values: $1\sigma$ to $6\sigma$ contour lines correspond to an ideal experiment with 4000 $W^+W^- \to \ell\nu q\bar{q}$ events. The contours are for A) no polarization; B) 70% transverse polarization, $2\phi$ modulation only; C) 70% transverse polarization, all observables; D) 50% longitudinal polarization of one beam. The dashed lines in (A) and (B) give the combinations of $\kappa_\gamma$ and $\kappa_Z$ for which $\mathfrak{M}_L$ and $\mathfrak{M}_R$, respectively, are as in the Standard Model.

the contour lines in Figs. 20 correspond to half the indicated sensitivity only, and hence a minor improvement of the measurement without beam polarization results. A transverse polarization of 50%–60% seems to be the minimal requirement.

### 4.5 Reduction of the number of free parameters

In view of the problems hidden in 'multidimensional regions' of parameter space, the authors of Ref. [8] suggested a conservative modification of the Standard Model which allows for only two free parameters. Underlying assumptions either have good empirical support from presently known electroweak interactions [conditions (i) and (ii)] or they are dictated by simplicity [constraints (iii) and (iv)]:

i) global SU(2) symmetry of weak interactions for $\alpha_{em} \to 0$;

ii) local $U(1)_{em}$ gauge invariance for $\alpha_{em} \neq 0$. This is implemented in the effective Lagrangian by minimal substitution, $\partial_\mu \to \partial_\mu + ieA_\mu$, by admitting $\gamma$–Z mixing and any further operators involving $F_{\mu\nu}$;

iii) only dimension-four operators are considered;

v) only operators which do not violate P or C are admitted (in fact this has only to be required for the $\gamma WW$ couplings).

Under these conditions, there are only two independent, free parameters left: an electroweak coupling $\hat{g}$ and $\varkappa$ ($\equiv \kappa_\gamma$). A measurement of the total cross-section of $e^+e^- \to W^+W^-$, and of the angular distribution of the W pairs at LEP II will constrain the parameters $\hat{g}$ and $\varkappa$ as shown in Figs. 21a to 21c [26]. Again one ends up with a banana-shaped region in the $\hat{g}$–$\varkappa$ plane reflecting the insensitivity of LEP II measurements (without polarization) to a correlated variation of the two parameters $\hat{g}$ and $\varkappa$.

[In the framework of an effective (cut-off) field theory, minimizing the degree of divergence of the one-loop contribution to the W mass leads to the relation [27] $\hat{g} = (e/\sin\theta_w)\varkappa$, which is still one step closer to the Standard Model. This relation largely removes the ambiguity in Fig. 21.]

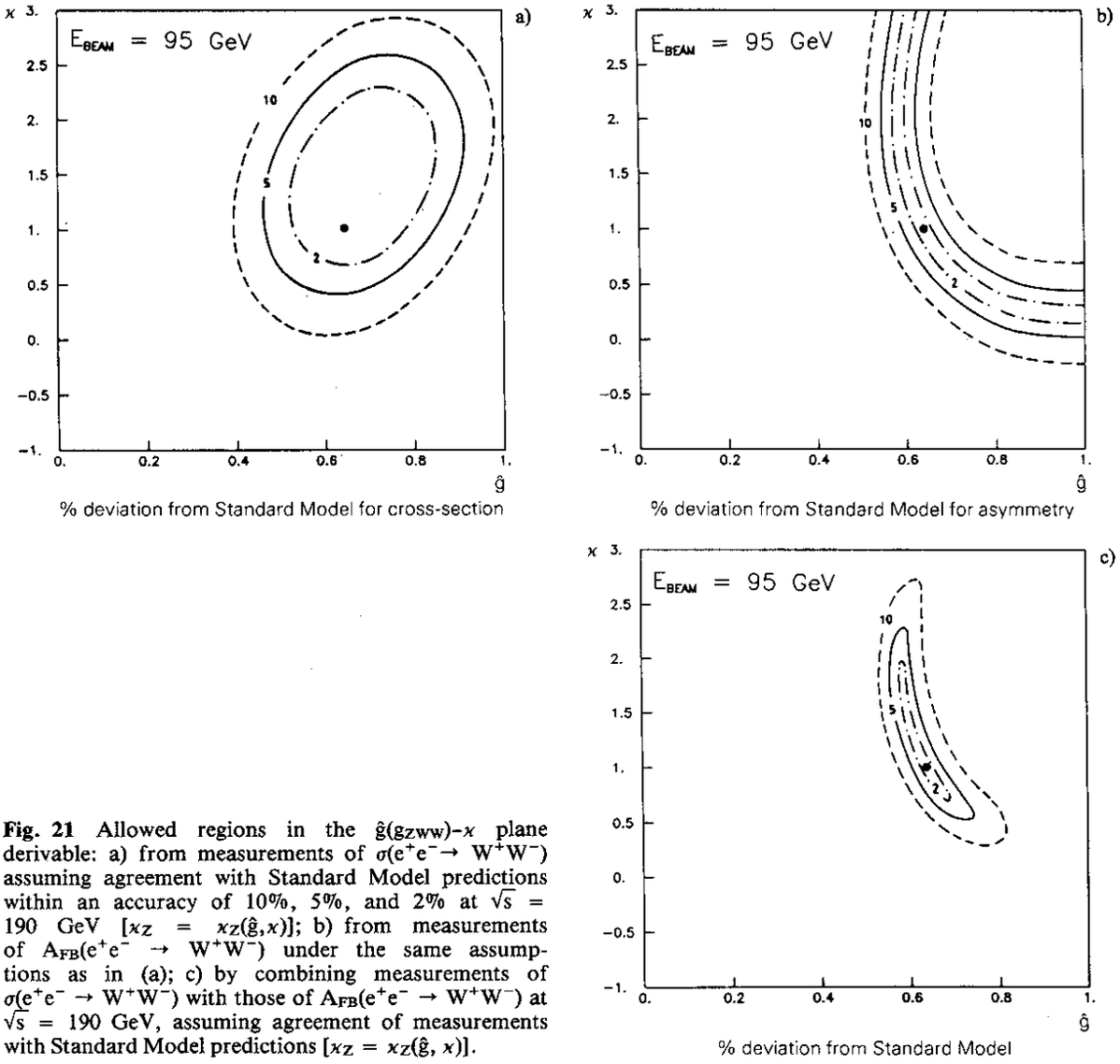


**Fig. 21** Allowed regions in the $\hat{g}(g_{ZWW})$-$\varkappa$ plane derivable: a) from measurements of $\sigma(e^+e^- \to W^+W^-)$ assuming agreement with Standard Model predictions within an accuracy of 10%, 5%, and 2% at $\sqrt{s}$ = 190 GeV [$\varkappa_Z = \varkappa_Z(\hat{g},\varkappa)$]; b) from measurements of $A_{FB}(e^+e^- \to W^+W^-)$ under the same assumptions as in (a); c) by combining measurements of $\sigma(e^+e^- \to W^+W^-)$ with those of $A_{FB}(e^+e^- \to W^+W^-)$ at $\sqrt{s}$ = 190 GeV, assuming agreement of measurements with Standard Model predictions [$\varkappa_Z = \varkappa_Z(\hat{g}, \varkappa)$].

## 5. HEAVY VECTOR BOSONS FROM NEARBY COMPOSITENESS

Next, let us turn to the issue of nearby compositeness, i.e. the concept of composite $W^*$,Z. Invoking the principle of vector dominance [28, 29], composite $W^*$,Z may be expected to imitate at low energies, $E \lesssim m_W$, the massive gauge bosons of the Standard Model. A clear-cut signature at higher energies is a possibly rich spectrum of further composites (at least some of them with masses $\lesssim$ 1 TeV).

In this section we focus on the most model-independent composites. First of all one expects excited states $W^{\pm *}$,$Z^*$ to be formed.

The most likely further composite ground state is an isoscalar vector boson, which indeed is predicted in most models of nearby compositeness. It is called Y if it couples to the weak hypercharge current, and $Y_L$ if it couples to its left-handed part only. A $Y_L$-type boson is, for example, predicted in the strongly coupled Standard Model to be discussed in Section 6.

Mass bounds from available data are

$$\begin{aligned} m_{W^*} &\gtrsim 220\ \text{GeV} \quad [30] \quad \text{for } g_{W^*} \geq g_W = 0.65 \\ M_Y &\gtrsim 350\ \text{GeV} \quad [14, 10] \\ M_{Y_L} &\gtrsim 260\ \text{GeV} \quad [14]\ . \end{aligned} \tag{29}$$

Thus we cannot expect them to be directly produced at LEP II, but have to rely on indirect manifestations, which fortunately turn out to be quite well defined.

The case study of a composite Y ($Y_L$) [28, 29, 31-33, 10] or a $W^{\pm *}$,$Z^*$ triplet [34-36] is indeed very interesting. First, each one introduces only a few unknown parameters into the effective low-energy theory for composite q, $\ell$, $W^\pm$, Z. Secondly, they influence the W, Z physics through Z-Y and Z-$Z^*$ mixing, respectively. Both properties are a consequence of the principle of vector dominance illustrated in Fig. 22.

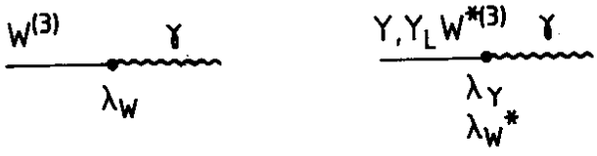


**Fig. 22** Vector dominance (mixing) for neutral vector bosons

For Y ($Y_L$) there are two new parameters: its mass $m_Y$ (before mixing) and its (universal) coupling $g_Y$ to $f\bar{f}$ pairs ($f = q,\ell$); the $\gamma$-Y mixing 'strength' $\lambda_Y$ is determined in terms of $g_Y$:

$$\lambda_Y = e/g_Y \ . \tag{30}$$

For $W^{\pm *}$, $Z^*$, there are three new parameters: $m_{W*}$ and $g_{W*}$ and a $\gamma$-$W^{0*}$ mixing parameter $\lambda_{W*}$ which is related to the corresponding $\gamma$-$W^0$ mixing parameter $\lambda_W$ by

$$e = \lambda_W g_W + \lambda_{W*} g_{W*} \ . \tag{31}$$

We shall discuss separately the effects of additional Y ($Y_L$) or $W^{\pm *}$, $Z^*$ bosons at LEP, following Refs. [10] and [36]. Since each of them influences both the Z mass and the Z couplings to $f\bar{f}$ pairs, it is first of all interesting to study their effect in $e^+e^- \to \mu^+\mu^-$ at LEP I, on top of the Z (assuming $m_W/m_Z$ to be provided by ACOL) without and with initial-state polarization. Then the additional potential of LEP II, provided by the lever arm of higher energies and an improved measurement of $m_W$, is explored, again without and with polarization. The results are finally presented as a sequence of increasingly tight boundary curves in a plot of squared mixing parameter $\lambda^2$ versus mass M of the new vector boson in question.

The influence of Y and $Z^*$ bosons in $e^+e^- \to W^+W^-$ production has also been studied (following Ref. [6]).

### 5.1 Isoscalar boson Y ($Y_L$) in $e^+e^- \to \mu^+\mu^-$ at LEP I/SLC and LEP II [10]

The effective Lagrangian that is relevant for $e^+e^- \to \mu^+\mu^-$ is given by [10]

$$\begin{aligned} \mathcal{L}_{Zf\bar{f}} &= Z_\mu \textstyle\sum_f \bar{f}\gamma^\mu 1/2\,(V_Z + A_Z\gamma_5)f \ , \\ \mathcal{L}_{Yf\bar{f}} &= Y_\mu \textstyle\sum_f \bar{f}\gamma^\mu 1/2\,(V_Y + A_Y\gamma_5)f \ , \end{aligned} \tag{32}$$

where the vector and axial-vector couplings $V_Z$, $A_Z$, $V_Y$, and $A_Y$ are functions of $m_W$, $m_Y$, $\lambda_W$, and $\lambda_Y$ which are detailed in Appendix 2; these functions are different for Y and $Y_L$. For completeness we also recall in Appendix 2 the masses $M_Z$ and $M_Y$ (after mixing), both also functions of $m_W$, $m_Y$, $\lambda_W$, and $\lambda_Y$ (which are the same for Y and $Y_L$).

Assuming $M_Z$ to be given, we considered four quantities which are sensitive to the presence of an additional Y ($Y_L$) boson: the mass ratio $m_W/M_Z$, the leptonic width of the Z boson, the forward-backward asymmetry $A_{FB}$, and the asymmetry $A_{LR}$ in case longitudinal beam polarization is available. The errors considered [10] to be sensible for the following analysis are

$$\delta(m_W/M_Z) = 0.002, \text{ very optimistically for ACOL, certainly feasible at LEP II,}$$
$$\delta\Gamma_{Z\to\ell^+\ell^-}/\Gamma_{Z\to\ell^+\ell^-} = 2\% \ ,$$
$$\delta A_{FB}(m_Z) = 0.01, \ \delta A_{FB}(190\ \text{GeV}) = 0.03 \ , \tag{33}$$
$$\delta A_{LR}(M_Z, 190\ \text{GeV}/c^2) = 0.02 \ .$$

The choice of errors on the asymmetries is intentionally conservative in view of the theoretical uncertainties of the Standard Electroweak Model on the one-loop level ($m_t$, $m_{Higgs}$) which serves as a reference model.

Figures 23a and 23b contain full information [10] on the sensitivity of LEP I/SLC and LEP II to an isoscalar boson of type $Y_L$; Fig. 23c and 23d display the same information for a Y-type boson. Many boundary curves in the

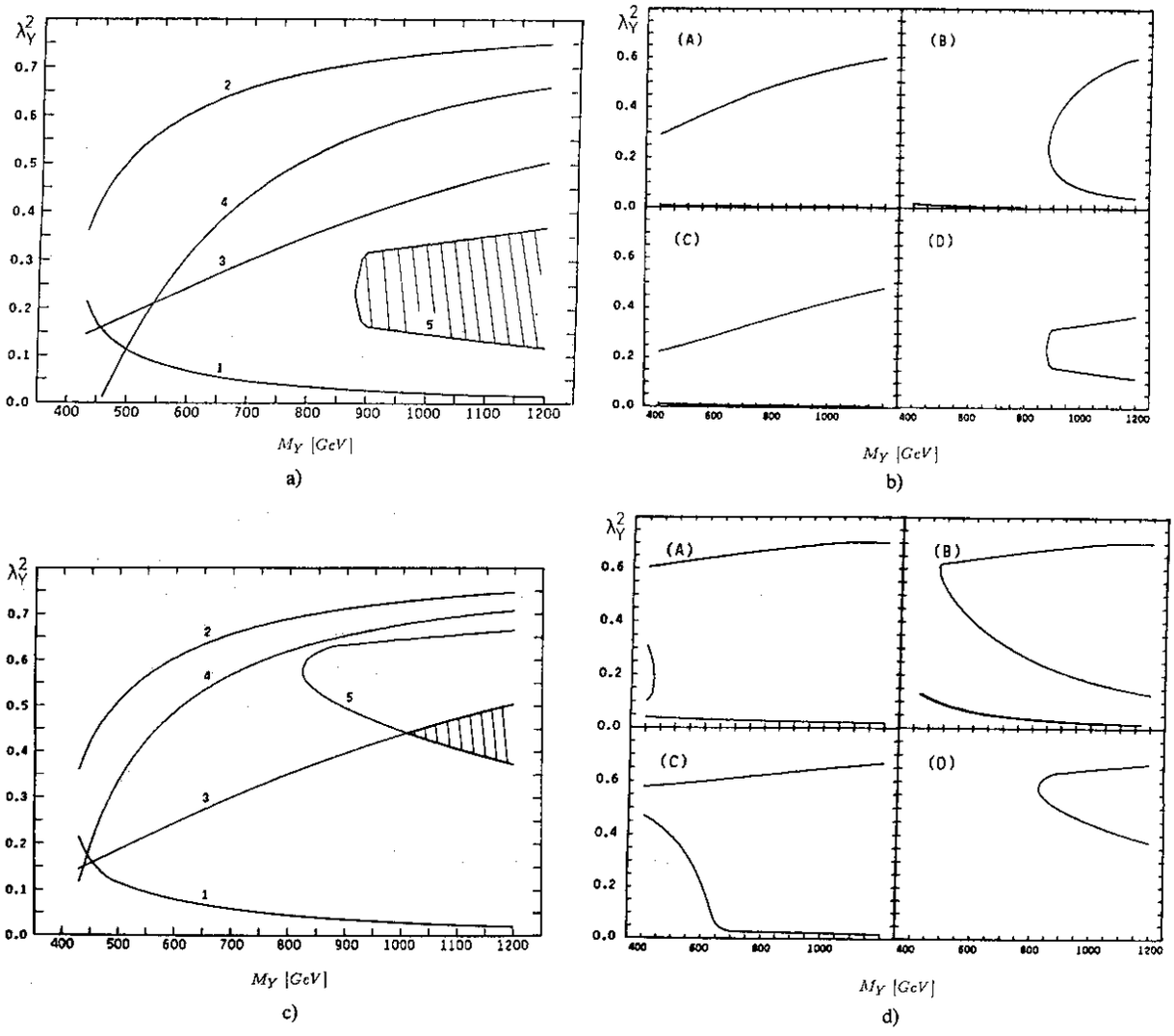


**Fig. 23**

a) Allowed region of the mixing parameter $\lambda_Y^2$ and the mass $M_Y$ of a $Y_L$ boson. Curves 1 and 2 are low-energy neutral-current constraints, curve 3 results from determining $m_W/M_Z$ to 0.2% accuracy, curve 4 from determining $\Gamma(Z \to \ell^+\ell^-)$ to 2% accuracy. Curve 5 summarizes the constraints from $A_{FB}$ and $A_{LR}$ which are detailed in Fig. 23b. The finally allowed region is the hatched region.

b) Allowed regions of $\lambda_Y^2$ and $M_Y$ for a $Y_L$ boson, based on measuring (A) $A_{FB}$ at $M_Z$, (B) $A_{FB}$ at $M_Z$ and 190 GeV, (C) $A_{FB}$ and $A_{LR}$ at $M_Z$, and (D) $A_{FB}$ and $A_{LR}$ at $M_Z$ and 190 GeV.

c) As in Fig. 23a, but for a Y boson.

d) As Fig. 23b, but for a Y boson.

plot $\lambda_Y^2$ versus $M_Y$ have a parabolic shape; this reflects the fact that large $\lambda_Y$ strongly modify the Z properties through mixing, and small $\lambda_Y$, i.e. large $g_Y$, give large Y ($Y_L$) contributions. This property also allows us to determine *absolute* bounds for $M_Y$ (and not for M/g as usual). The most sensitive quantities are i) $m_W/M_Z$ and in particular ii) the electroweak asymmetries $A_{FB}$ and $A_{LR}$, which provide a decisive reduction of the allowed region in the $\lambda_Y^2$-$M_Y$ plane.

Whilst LEP I/SLC will push the absolute mass bounds [10] up to

$$M_Y \gtrsim 600 \text{ GeV} , \quad M_{Y_L} \rangle 500 \text{ GeV} , \tag{34}$$

at LEP II the corresponding bounds [10] are

$$\begin{aligned} &M_Y \gtrsim 720 \text{ GeV} , \quad M_{Y_L} \gtrsim 900 \text{ GeV} , \quad \text{without initial-state polarization,} \\ &M_Y \gtrsim 1 \text{ TeV} , \quad M_{Y_L} \gtrsim 900 \text{ GeV} , \quad \text{with } A_{LR} \text{ measurement.} \end{aligned} \tag{35}$$

Thus, even with conservative errors on the asymmetries, LEP II is able to essentially exclude masses below 1 TeV. Theoretically, masses above 1 TeV for ground-state composite partners of $W^\pm$, Z are very unlikely. In conclusion, LEP II has the potential to confirm or rule out an isoscalar partner of composite $W^\pm$,Z.

### 5.2 Excited $Z^*$ bosons in $e^+e^- \to \mu^+\mu^-$ at LEP I/SLC and LEP II

An analogous analysis [36] has been carried out for the excited $W^{\pm *}$,$Z^*$ bosons. The starting position is, however, more complicated: there is one more free parameter and, besides the neutral-current sector, also the charged-current sector is affected. In order to present the results in a meaningful way, one of the parameters, say $\lambda_{W^*}$, has been replaced [35, 36] by a new one, n, defined by

$$\lambda_{W^*} = \lambda_W (m_W/m_{W^*})^n . \tag{36}$$

The point is that from analogy to strong interactions one has some prejudice about the range of reasonable values for n: n = 1 corresponds to the constraint of local duality and n = 3/2 results from a bound-state model with linearly rising confining potential.

The final result [36] of the analysis, again assuming $m_W$, $M_Z$, $\Gamma_{Z\to\ell^+\ell^-}$, $A_{FB}$ ($M_Z$, 190 GeV) and $A_{LR}$ ($M_Z$, 190 GeV) to be measured with the accuracies (33), is presented in Fig. 24. It shows the allowed region in the

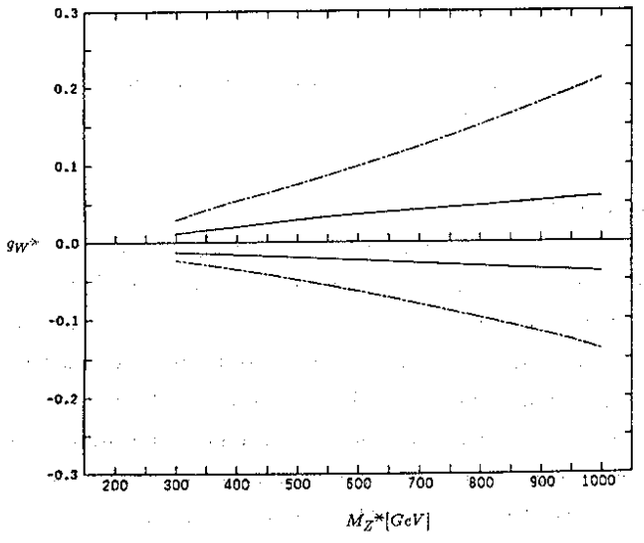


**Fig. 24** Allowed region in coupling $g^*$ and mass $m_{W^*}$ of an excited triplet $W^{*\pm}$,$Z^*$ of vector bosons, assuming $A_{FB}$ and $A_{LR}$ measurements at $\sqrt{s} = m_Z$ and 190 GeV. Solid line, n = 1; dash-dotted line, n = 1.5 (see text). The allowed regions are between the two respective branches.

$g_{W^*}$–$M_{Z^*}$ plane for the two representative values of the third parameter n: n = 1 and n = 3/2. Except for very small couplings, the combined LEP I/SLC and LEP II reach for excited $Z^*$ is again of the order of 1 TeV.

### 5.3 Heavy vector bosons in $e^+e^- \to W^+W^-$

Following Ref. [6] we also discuss the effect of a Y and $Z^*$ on $e^+e^- \to W^+W^-$. Maximal effects are achieved for 'left-type' bosons, $Y_L$ and $Z^*_{(L)}$.

With the following ansatz [6] for the YWW coupling

$$\mathcal{L}_{YW^+W^-} = -g_{YWW}\,\epsilon^{\mu\nu\varrho\sigma}\,Y_\mu\,(\partial_\sigma \vec{W}_\nu \cdot \vec{W}_\varrho - \vec{W}_\nu \cdot \partial_\sigma \vec{W}_\varrho)\ , \tag{37}$$

and the assumption of strong coupling, essentially $g^2_{YWW} \simeq 4\pi$, the angular distribution in $e^+e^- \to W^+W^-$ is modified as shown in Fig. 25 for a $Y_L$ boson. The apparent sensitivity to masses $m_Y$ of the order of 600 GeV has to be rescaled, from strong coupling ($g \approx \sqrt{4\pi}$) to weak coupling ($g \approx 0.65$). The resulting reach at LEP II is then about 200 GeV, which cannot compete with the bounds of the order of 1 TeV obtained from $e^+e^- \to \mu^+\mu^-$.

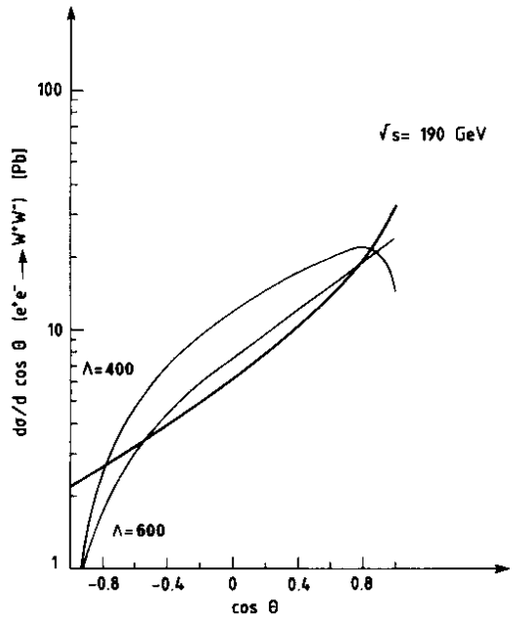


**Fig. 25** Effect of a $Y_L$ boson on $e^+e^- \to W^+W^-$ angular distribution at $\sqrt{s}$ = 190 GeV, for $\Lambda$ = 400 and 600 GeV, and for $g^2/4\pi = 1$ (corresponding to $M_Y \approx 100$ GeV for $g_Y \approx g_W = 0.65$).

### 5.4 Vector bosons from a strongly interacting Higgs sector [37]

Another potential source of a new triplet of heavy vector bosons, called $V^{\pm,0}$, is a strongly interacting Higgs sector. To first approximation it will be hard to distinguish them experimentally from excited composite $W^*$, $Z^*$.

In the standard electroweak model the Higgs sector is largely regarded as an effective theory valid for an energy below a scale of the order of 1 TeV. Regardless of the underlying theory, the Higgs sector is associated with a scale of the order of 1 TeV related to the breaking of perturbative unitarity, which means that if the mass of the Higgs is greater than that threshold the Higgs sector loses its perturbative character and acquires the features of a strongly coupled theory. Therefore new phenomena are expected and new high-energy predictions are made for the electroweak model. The existence of bound states with J = 0 [38] and J = 1 [39] has been conjectured.

The new triplet of vector bosons $V^{\pm,0}$ [39] has mass $m_V$ and gauge coupling constant $g''$. For $g'' \to \infty$, $m_V \to \infty$ and one recovers the Standard Model. The couplings of the new vector bosons to quarks and leptons are of the order of $g/g''$. It has been checked that the low-energy phenomenology of the Standard Model is not significantly modified even for relatively low values of $m_V$.

Accurate measurements of $m_W$ and $m_Z$ will provide sensitive tests. In fact the relation $m_W$ as a function of $m_Z$, which is independent of the Weinberg angle, is modified in this model by the existence of the new vector bosons, to become

$$(1 - m_W^2/m_Z^2)^{1/2} m_W = [\pi\alpha(m)/\sqrt{2}\, G_F]^{1/2} [1 + (g/g'')^2 + 1/2 \cdot (g/g'')^2 (m_W^2/m_V^2)] , \qquad (38)$$

where $m \approx m_W$ is a renormalization scale and the bulk of the radiative corrections is taken into account by the running $\alpha(m)$. This test is essentially independent of $m_V$.

Figure 26a shows the predicted forward-backward asymmetry in $e^+e^- \to \mu^+\mu^-$ for $m_W = 250$ GeV and different values of $g/g''$. In Fig. 26b the asymmetry at the Z resonance is plotted versus $g/g''$ for two different values of $m_V$.

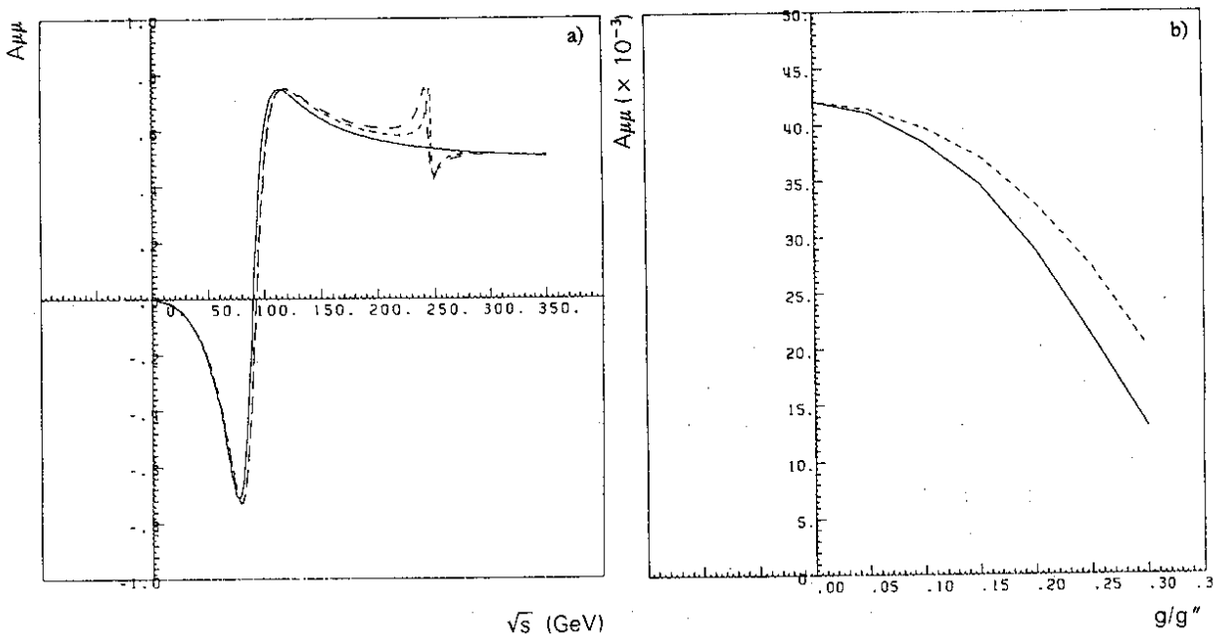


**Fig. 26** a) Effect of a vector boson bound state of mass $m_V = 250$ GeV, as may be expected from a strongly interacting Higgs sector on the forward-backward asymmetry in $e^+e^- \to \mu^+\mu^-$ for different couplings: Standard Model (solid), $g/g'' = 0.16$ (short-dashed), $g/g'' = 0.22$ (long-dashed). b) Forward-backward asymmetry at the Z resonance versus the coupling for $m_V = 200$ GeV (solid) and 250 GeV (dashed).

## 6. EXOTIC ISOSCALAR BOSONS FROM THE STRONGLY COUPLED STANDARD MODEL [11]

The strongly coupled Standard Model (SCSM) [40, 41] is a consistent candidate model for nearby compositeness and thus a respectable competitor for the Standard Model. It mimics Standard Model physics at energies below the Fermi scale ($E \lesssim m_W$); at higher energies it predicts a rich spectrum of composite isoscalar bosons, mostly with exotic quantum numbers.

The SCSM is intimately related to the Standard Model: it starts from the same SU(2) × U(1) gauge Lagrangian, involving 12 left-handed fermion doublets $\psi_L$ and a complex scalar doublet $\phi$. However, the theory is

evaluated in the phase where SU(2) is not spontaneously broken, i.e. it is confining. The confinement scale—the energy at which the SU(2) gauge coupling becomes large—is arranged to be of the order of the weak interaction scale. The doublets $\psi_L$ and $\phi$ thus play the role of preons, and the physical particle spectrum consists of SU(2)-singlet bound states. Left-handed quarks and leptons appear as bound states of $\psi_L$ and $\phi$, the triplet $W^{\pm}$ and Z, and a scalar Higgs-like boson as composites of two $\phi$'s.

From the 12-plet of fermionic preons $\psi_L$, new SU(2)-singlet bound states can be formed, all of them isoscalar weak bosons:

i) a 144-plet of $\psi_L\dot{\psi}_L$-type vector bosons V (spin 1);

ii) 144 bosons of the type $\psi_L\psi_L$, a 78-plet of spin-1 bosons K, and a 66-plet of spin-0 bosons S.

The V multiplet contains colour-octet and colour-singlet bosons, and colour-triplet leptoquarks of charge $^2/_3$; a combination of the colour-singlet bosons has the quantum numbers of the $Y_L$ boson discussed in Section 5. The K and S multiplets contain colour-triplet leptoquarks of charge $-^1/_3$, dileptons of charge $-1$, and colour sextet and antitriplets of diquarks. Each of the three multiplets enters the effective (weak) interactions with quarks and leptons with only two parameters, a mass and an effective coupling.

A remarkable property of this model is that even though individually many of these bosons contribute to flavour-changing neutral currents, in the sum these contributions *cancel*. For this reason, lower mass bounds from present data are again in the 250–500 GeV mass range, depending on the couplings.

The V multiplet contributes to $e^+e^- \to e^+e^-$, $e^+e^- \to \mu^+\mu^-$, and $e^+e^- \to q\bar{q}$, and particularly strongly to quarks with charge $-^1/_3$, which may be isolated in the case of the $b\bar{b}$ final state. These contributions are calculable in terms of two parameters, $g_V$ and $m_V$. The predictions at LEP II energies as a function of $m_V$ were worked out [11], assuming

$$g_V = 1 \ . \tag{39}$$

[This is a compromise between $g_V \approx O(g_W)$ with $g_W = 0.65$, and $g_V > g_{colour}$ at $E \approx m_V$, which is necessary if colour gauge interactions are to be treated as corrections to weak interactions at these energies.] We further simplify by disregarding mixing with the photon and assuming U(12) instead of SU(12) symmetry.

We ignore possible effects due to the S and K bosons. They contribute only to $e^+e^- \to q\bar{q}$ by leptoquark exchange, the K contribution is suppressed at energies well below $m_K$ and, last but not least, four additional parameters would have to be handled.

The relevant diagrams [11] for the exotic V-boson contributions to $e^+e^- \to e^+e^-$, $\mu^+\mu^-$, $b\bar{b}$ are shown in the left upper corner of Figs. 27a–27c. In all three cases there is a crossed-channel exchange contribution; in $e^+e^- \to b\bar{b}$ it is a leptoquark exchange. A direct channel $Y_L$-type exchange contributes only to $e^+e^- \to e^+e^-$. Given our simplifications, the $Y_L$ completely decouples from 'off-diagonal' channels $e^+e^- \to \mu^+\mu^-$, $q\bar{q}$; in a more realistic evaluation its contribution will be non-vanishing, but strongly suppressed. This result is a peculiarity of the SCSM [due to the large SU(12) or U(12) global symmetry].

Figures 27a to 27c show the effects of the exotic exchanges on $e^+e^-$, $\mu^+\mu^-$, and $b\bar{b}$ final states. The theoretical calculation was performed without radiative corrections. However, we feel that an inclusion of these corrections would not alter our conclusions. In the upper right-hand corners the expected deviations from the Standard Model at $\sqrt{s} = 190$ GeV are displayed, compared with the expected experimental error on the corresponding process; these include statistical and systematic errors and a conservative estimate for the b-tagging efficiency.

LEP II is clearly sensitive to the exotic isoscalar composites up to masses of the order 1–1.5 TeV. This makes LEP II a decisive tool for ruling out or confirming the SCSM. Firstly, in this model with a confinement scale of the order of 250 GeV, masses of ground-state composites above 1 TeV seem unlikely. Secondly, the correlations of the predicted signals in *three different* $e^+e^-$ reactions (e.g. positive deviation in $e^+e^- \to e^+e^-$, negative deviations in $e^+e^- \to \mu^+\mu^-$, $b\bar{b}$, etc.) strongly enhance the potential of LEP II to settle the issue.

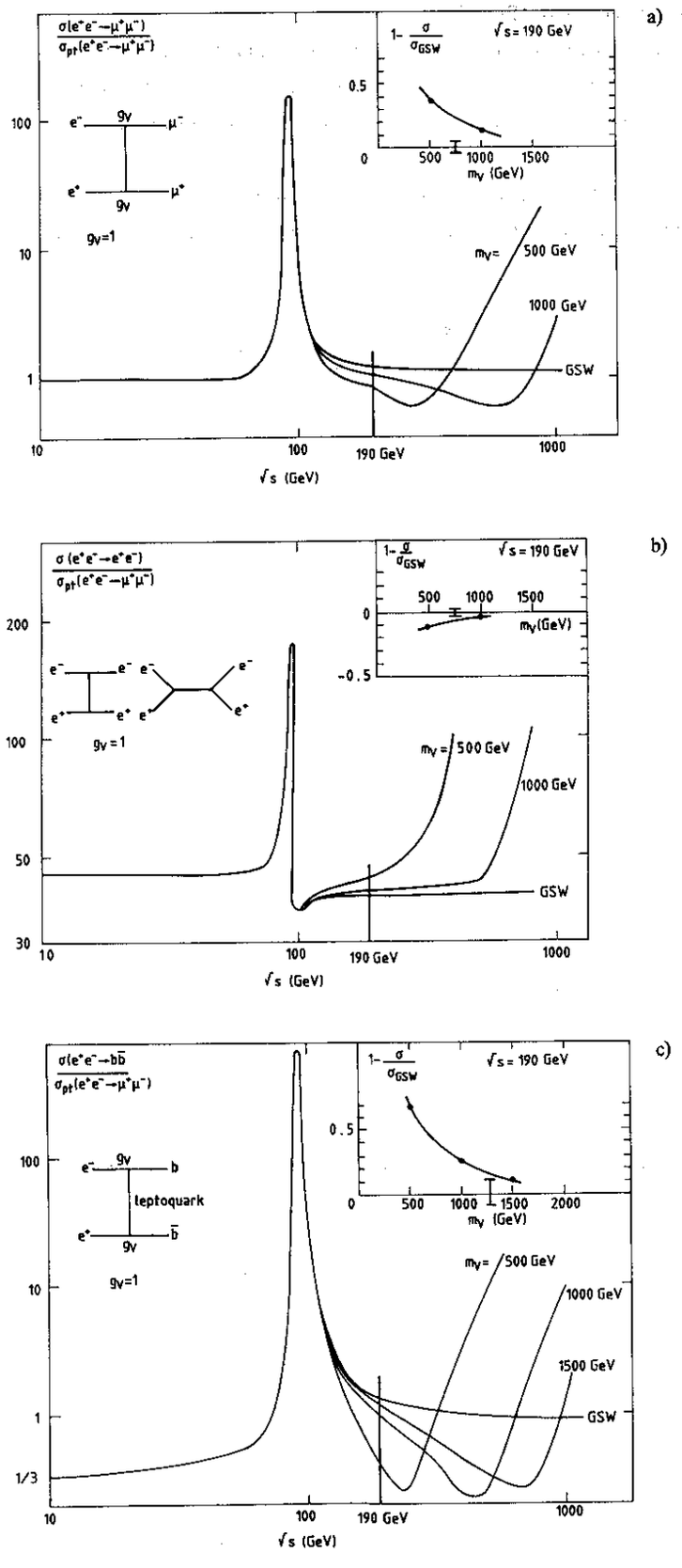


**Fig. 27** Correlated effects of exotic isoscalar vector bosons on $\mu^+\mu^-$(a), $e^+e^-$(b), and $b\bar{b}$ (c) final states, as expected in the strongly coupled Standard Model, assuming a coupling g = 1. The insets show the experimental sensitivity at $\sqrt{s}$ = 190 GeV (Ref. [11]).

## 7. FURTHER COLOURED COMPOSITES

Some subconstituents of composite quarks and leptons will have to carry colour; quite generally this leads to the prediction of further coloured composites. Typical examples, among them leptoquarks, have been discussed already in the context of the SCSM. We have focused on two further examples of particular interest for LEP II physics:

i) Colour octet electrons [42], a safe expectation if the electron has coloured constituents. They could manifest [2, 43] themselves by a t-channel contribution to the process $e^+e^- \to gg$ (see Fig. 28).

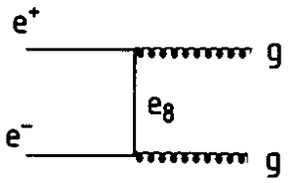


**Fig. 28** The exchange of a colour-octet electron in $e^+e^- \to gg$

ii) Light leptoquarks which could be pair-produced at LEP II. Leptoquarks as light as this can only survive [44] the tight bounds on flavour-changing neutral currents if they are (pseudo-)Goldstone bosons (spin 0) with characteristically small couplings to light quark-lepton pairs. Mechanisms which are potential sources of such light leptoquarks have been discussed in Ref. [44].

### 7.1 The $e_8$ exchange in $e^+e^- \to gg$

The appropriate chirality-conserving, CP-conserving, gauge-invariant coupling is [2, 43]

$$(g_s/2\Lambda)\,\bar{\psi}^a_{\ell_8}\,\sigma^{\mu\nu}\,G^a_{\mu\nu}(c - d\gamma^5)\,\psi_\ell + \text{h.c.}, \tag{40}$$

where $c = \pm d$, $g_s^2/4\pi = \alpha_{QCD}$, and $G^a_{\mu\nu}$ is the gluon field-strength tensor.

The resulting cross-section is:

$$\frac{d\sigma}{dt} = 8\pi\alpha_s^2\,(c/\Lambda)^4\ \ \frac{16tu}{s^2}\ \{[t/(m^2_{e_8} - t)]^2 + [u/(m^2_{e_8} - u)]^2\}\ . \tag{41}$$

The important feature is the $\sin^2\theta$ dependence of the process, which is quite distinct from the angular distribution of the Standard Model $e^+e^- \to q\bar{q}$ background. A Monte Carlo simulation [45] shows that indeed at large angles ($-\frac{1}{3} < \cos\theta < \frac{1}{3}$) an $e^+e^- \to gg$ cross-section of 1 to 1.5 pb should be observable. We assume that one third of the $q\bar{q}$ background could be rejected by flavour tagging. From a fit (Fig. 29) the following bound is obtained:

$$\Lambda m_{e_8}/c \geqslant 2 \times 10^5\ \text{GeV}^2\ , \tag{42}$$

which for $c = 1$ and $\Lambda = m_{e_8}$ leads to a bound

$$m_{e_8} > 450\ \text{GeV}/c^2\ . \tag{43}$$

We examined the possibility of using polarization to improve the bounds and found that, whilst it is of little use for proving the existence of the effect, it could give information once a signal has been found.

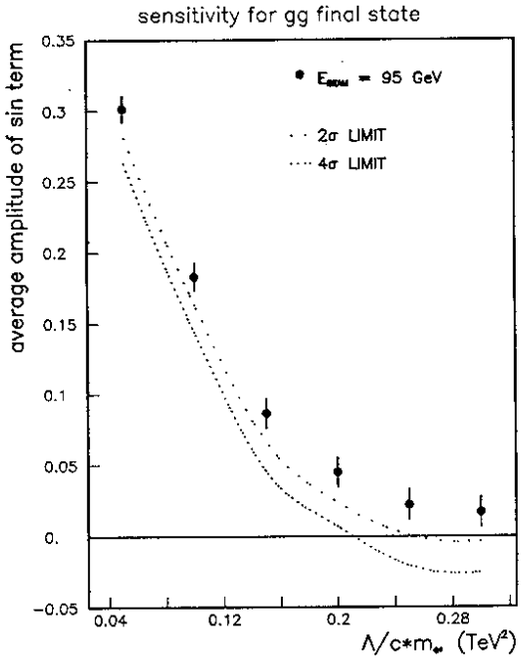


**Fig. 29** Bound on the mass of a colour-octet electron, as obtained from an angular fit to the reaction $e^+e^- \to 2$ jets

Potentially, gluon bremsstrahlung could destroy the event orientation and ruin the identification, but it was found to be quite tolerable. The limit given above is somewhat lower than the one found in Ref. [2]. This results from the more realistic nature of our Monte Carlo study.

### 7.2 Light leptoquarks

In the most likely realization [44], light leptoquarks have the following properties: a mass of $O(\sqrt{\alpha_c/\pi}\,\Lambda) \approx O(40\ \text{GeV})$, charge 2/3 and decay modes

$$\begin{aligned} \chi &\to q_{-1/3}\,\ell^+ \ , \\ &\to q_{2/3}\,\bar{\nu} \ ; \end{aligned} \tag{44}$$

and very small partial decay widths

$$\Gamma \approx [O(1)/4\pi] m_\chi\,(m_q^2 + m_\ell^2)/\Lambda^2 \ , \tag{45}$$

with $\Lambda \approx (\sqrt{2}\,G_F)^{-1/2} \approx 250$ GeV. Nothing is known about whether a single $\chi$ is more likely, which would preferentially decay into the heaviest accessible $q\bar{\ell}$ pair or, for example, one $\chi$ per generation. We investigate the latter possibility and assume a light first-generation leptoquark $\chi^{(1)}$ decaying into a) $de^+$, or b) $u\bar{\nu}_e$. Mode (a) provides isolated electrons, mode (b) provides jets and missing energy. Monte Carlo simulations were made [46] for leptoquark pair-production, $e^+e^- \to \gamma \to \chi\bar{\chi}$, leading to all three final states

$$\begin{aligned} &\text{i)}\ e^+ + e^- + \text{jets} \ , \\ &\text{ii)}\ e^\pm + \text{jets} + \not{E} \ , \\ &\text{iii)}\ \text{jets} + \not{E} \ , \end{aligned} \tag{46}$$

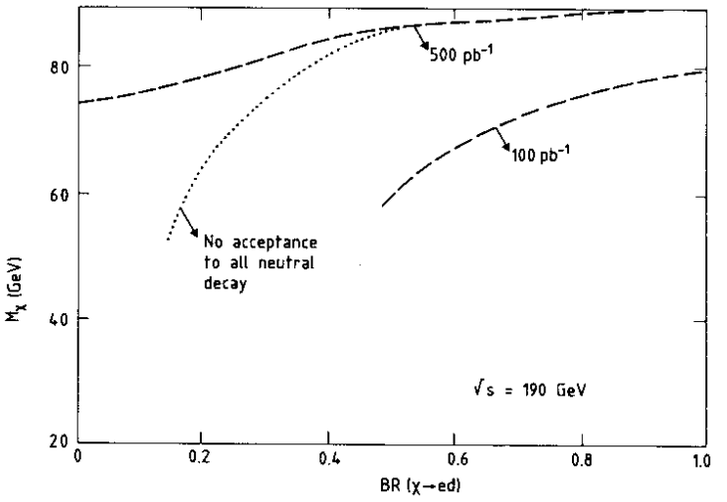


**Fig. 30** Accessible mass bound of pair-produced (spin-0) leptoquarks

and their visibility over background was studied. The result is shown in Fig. 30, where the mass of the accessible leptoquark is given as a function of the branching ratio of $\chi \rightarrow$ ed. With hermetic calorimetry and acceptance to all neutral modes, it should be possible to detect $\chi$'s up to $\approx$ 80 GeV, independently of the branching ratio into ed.

## 8. RARE MODES OF THE Z

Since a large luminosity will be accumulated on the Z, we have tried to find out what could be learnt there about compositeness and have studied the visibility of rare decay modes of the Z [9].

### 8.1 $Z^0 \rightarrow 3\gamma$

The branching ratio is $\approx 7.7 \times 10^{-10}$ in the Standard Model. In a composite model the process of Fig. 31, independently of the colour content of the constituents, leads to a higher branching ratio. To be quantitative in this respect is difficult because one needs a bound-state model of the Z from unknown constituents. 'Guestimates' [47] lead to $Br(3\gamma) \approx 5 \times 10^{-5} Q_c^4$, where $Q_c$ is the mean electric charge of the constituents.

The background is due to the ee $\rightarrow \gamma\gamma$ process with a hard $\gamma$ bremsstrahlung and was simulated according to Berends and Kleiss [22]. Appropriate cuts were performed to enhance the ratio of the signal, generated according to phase space, over background. The mass distribution for $2\gamma$ systems is displayed in Fig. 32.

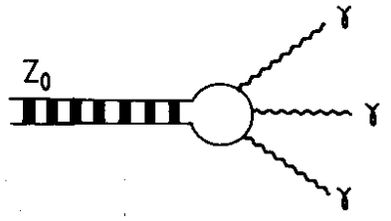


**Fig. 31** $Z \rightarrow 3\gamma$ in a composite model

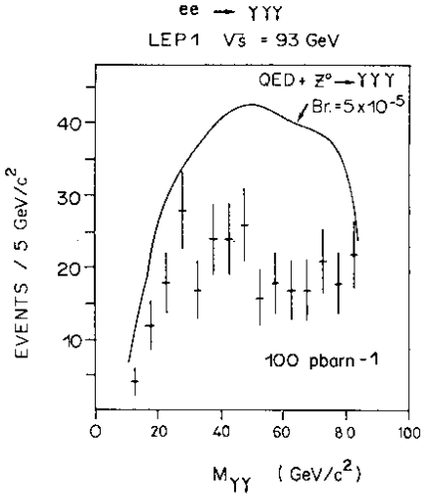


**Fig. 32** Distribution of $2\gamma$ mass from the QED process $e^+e^- \rightarrow 3\gamma$ at LEP I (error bars). The curve shows the effect of a non-standard decay $Z \rightarrow 3\gamma$.

The conclusion is that, with a systematic error of 3% on the luminosity and an exposure of 100 events per picobarn, the $3\gamma$ mode will be visible if its branching ratio is larger than $1.1 \times 10^{-5}$ (95% CL).

### 8.2 $Z \to \mu\mu\gamma$

The background is radiative muon pair production. Quite efficient cuts on the $\mu$–$\gamma$ angle and on the $\mu^+\mu^-$ effective mass can be performed against background, with the result [9] that the mode should be visible if its branching ratio is above $10^{-5}$. A model for the signal would be needed in order to get a more precise answer.

If no signal is observed in either one of these decay modes, we will be unable to draw conclusions about Z compositeness, since the predictions are so doubtful. On the other hand, even though no precise parameter could be derived from a positive result, the observation of a signal would be crucial information.

## 9. CONCLUSIONS

A first important issue was to determine the *reach* of LEP II for first signals of compositeness and to put it into perspective with the reach of LEP I/SLC and of PETRA/PEP.

From $e^+e^- \to e^+e^-, \mu^+\mu^-$ at LEP II, bounds on the compositeness scale of contact interactions of the order of

$$\Lambda \gtrsim 4\text{–}13 \text{ TeV} \tag{47}$$

may be obtained, assuming strong coupling, $g = \sqrt{4\pi}$. The precise numerical value depends on the helicity structure of the contact term. These bounds agree with those obtained on masses of various virtually exchanged particles, such as excited electrons, isoscalar bosons Y, excited Z-bosons $Z^*$, leptoquarks, colour octet leptons, etc.,

$$m \gtrsim 0.5\text{–}1.5 \text{ TeV} , \tag{48}$$

based on the assumption of weak coupling, $g \approx g_W \approx 0.65$ or $g \approx e$. (The rescaling factor is $\sqrt{4\pi}/0.65 \approx 5.5$ or $\sqrt{4\pi}/e \approx 11$, respectively). The precise numerical value of the mass bound depends on the quantum numbers of the exchanged particle.

We point out that the determination of our bounds includes realistic (statistical and systematic) errors, detector performances, and, if relevant, realistic background estimates. More naïve bounds would come out roughly twice as large. This should be kept in mind when comparing the LEP II reach (47), (48) for compositeness with first 'guestimates' for the reach of $p\bar{p}$ colliders or HERA.

Let us mention that in the context of the reach for compositeness, i) a *moderate* increase in luminosity does not significantly improve the result (reach $\propto \sqrt[4]{\int L\, dt}$), ii) the technical and financial effort for a *small* gain in $\sqrt{s}$, say of the order of 10 GeV, is not worth while (reach $\propto \sqrt{s}$).

To first approximation the reach for compositeness is proportional to $\sqrt{s}$ (for $\sqrt{s} \neq m_Z$). Correspondingly the reach of LEP II is about four times the one attainable at PETRA/PEP. This rule of thumb does not apply to a measurement on top of the Z at LEP I/SLC: the sensitivity to a real contact interaction term is considerably reduced owing to the lack of interference with the imaginary Standard Model amplitude. As a result the LEP II reach is again roughly four times the one of LEP I/SLC. However, measurements on top of the Z may provide complementary information: e.g. by a search for anomalous decay modes of the Z or by a search for mixing effects with neutral vector bosons such as, for example, an isoscalar Y or an excited $Z^*$, giving rise to modifications of the Z mass and couplings.

A second important issue is the new channel $e^+e^- \to W^+W^-$, open at LEP II. It provides the unique opportunity to probe the triple boson vertices $W^+W^-Z$ and $W^+W^-\gamma$ for deviations from the Standard Model due to compositeness. This is completely novel ground; the search for compositeness effects in $e^+e^- \to W^+W^-$ may be considered to be complementary to the one performed in four-lepton interactions. Deviations from the Standard

Model predictions at the 10% to 20% level will be observable, apart from certain unfavourable correlations of couplings. In order to reach this level of precision, an exposure of $\approx$ 500 pb$^{-1}$ is needed, which represents a long programme of at least two years. In view of the unique potential of the $W^+W^-$ channel, an increase in luminosity is strongly advocated.

A clear-cut conclusion is reached for the issue of nearby compositeness: LEP II will at least be able to seriously corner the concept of composite $W^\pm$, Z bosons, or even to settle the issue. (Instrumental is, for example, the search for a composite isoscalar partner Y or an excited $Z^*$.) Furthermore, LEP II measurements will either confirm or rule out the strongly coupled Standard Model, a prominent candidate model for nearby compositeness.

An investigation of the possible benefit of beam polarization for the compositeness search at LEP II leads us to the following intricate conclusion*):

i) Polarization does not significantly increase the *maximum* reach of LEP II for *first* signals of compositeness; however, longitudinal polarization strongly boosts the reach for contact interactions with otherwise unfavourable helicity combinations (or, equivalently, for new particles with otherwise unfavourable couplings).

ii) However, once signals of new physics are found, polarization will be of *crucial importance for pinning down* these effects. Its analysing power for deciding whether new effects are due to compositeness and, if so, which of the many possible phenomena in the large 'ballpark compositeness' is at work, has shown itself repeatedly in this report. Examples are the power to disentangle contributions from several anomalous WWZ and WW$\gamma$ couplings in $e^+e^- \to W^+W^-$, or the power to pin down effects due to isoscalar Y and $Z^*$ with masses in the 1 TeV range.

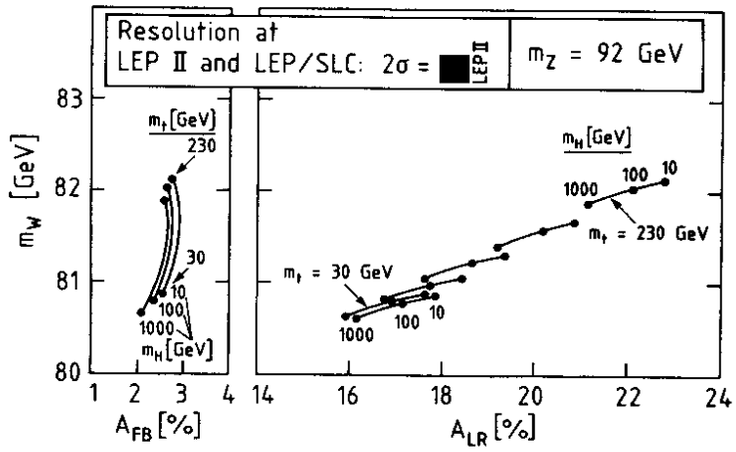


**Fig. 33** Comparison of the sensitivity to top and Higgs masses obtained from the W mass measurement (LEP II) and asymmetry measurement (LEP I/SLC) without (left) and with (right) longitudinal polarization. To guide the eye, all scales are normalized to the expected experimental errors (from Ref. [3]).

Finally, we consider the LEP detectors, as they are planned for LEP I, to be quite adequate for the physics discussed in this report.

**Acknowledgements**

We thank M. Placidi (LEP) for a very informative discussion on polarization. We warmly thank the Text Composition Service of CERN for their very efficient processing of the manuscript.

---

*) Let us emphasize, however, that this conclusion has no bearing on the fact that longitudinal beam polarization at LEP I is absolutely vital for a sensitive test of the Standard Model, as is illustrated comprehensively in Fig. 33 [3].

## REFERENCES


[1] R.D. Peccei, DESY preprint 86-138 to appear in Proc. 23rd Int. Conf. on High-Energy Physics, Berkeley, 1986.

[2] G. Barbiellini et al., *in* Physics at LEP, eds. J. Ellis and R.D. Peccei (CERN 86-02, Geneva, 1986), Vol. 2, p. 1.

[3] F. Schrempp, Max-Planck-Inst. Munich preprint MPI-PAE/PTh 69/86 (1986), to appear in Proc. 23rd Int. Conf. on High-Energy Physics, Berkeley, 1986.

[4] E.J. Eichten, K.D. Lane and M.E. Peskin, Phys. Rev. Lett. **50**, 811 (1983).

[5] B. Schrempp, F. Schrempp, N. Wermes and D. Zeppenfeld, preprint CERN-EP/87-34 (1987), submitted to Nucl. Phys. B.

[6] P. Méry, M. Perrottet and F.M. Renard, Marseilles preprint CPT-86/P 1919 (1986) and Montpellier preprint PM/86-23 (1986).

[7] K. Hagiwara, R.D. Peccei and D. Zeppenfeld, DESY preprint 86-058 (1986).

[8] M. Kuroda, J. Maalampi, D. Schildknecht and K.H. Schwarzer, Bielefeld preprint BI-TP 86/27 (1986) and Nucl. Phys. **B284**, 271 (1987).

[9] D. Bloch, Strasburg preprint CRN-HE 86-08 (1986).

[10] U. Baur, M. Lindner and K.H. Schwarzer, Max-Planck-Inst. Munich preprint MPI-PAE/PTh 74/86 (1986).

[11] B. Schrempp and F. Schrempp, preprint in preparation.

[12] M.E. Peskin, Proc. Int. Symp. on Lepton and Photon Interactions at High Energies, Bonn, 1981, ed. W. Pfeil (Univ. Bonn, 1981), p. 800.

[13] W. Buchmüller, Lectures given at Schladming, 1985, Acta Phys. Austriaca Suppl. **27**, 517 (1985).

[14] B. Schrempp, Max-Planck-Inst. Munich preprint MPI-PAE/PTh 72/86, to appear in Proc. 23rd Int. Conf. on High-Energy Physics, Berkeley, 1986, and MPI-PAE/PTh.17/87 preprint to appear in Proc. 6th Topical Workshop on Proton-Antiproton Physics, Aachen, 1986.

[15] D. Wyler, to appear in Proc. 23rd Int. Conf. on High-Energy Physics, Berkeley, 1986.

[16] See, for example, S. Komamiya, to appear in Proc. Int. Symposium on Lepton and Photon Interactions at High Energies, Kyoto, 1985.

[17] K. Hagiwara, S. Komamiya and D. Zeppenfeld, Z. Phys. **C29**, 115 (1985).

[18] N. Cabibbo, L. Maiani and Y. Srivastava, Phys. Lett. **139B**, 459 (1984).

[19] a) F.A. Berends and R. Kleiss, Nucl. Phys. **B228**, 537 (1983).
b) F.A. Berends, R. Kleiss and S. Jadach, Comput. Phys. Commun. **29**, 185 (1983).

[20] H.J. Behrend et al., Phys. Lett. **168B**, 420 (1986).

[21] D. Zeppenfeld, internal note to the Working Group.

[22] F.A. Berends and R. Kleiss, Nucl. Phys. **B186**, 22 (1981).

[23] F.E. Low, Phys. Rev. Lett. **14**, 238 (1965).
A. Litke, Ph.D. Thesis, Harvard Univ. (1970), unpublished.

[24] E. Longo, contribution to this Conference.

[25] D. Zeppenfeld, DESY preprint 86-123 (1986).

[26] K. Hamacher, internal note to the Working Group.

[27] H. Neufeld, D. Schildknecht and J. Stroughair, preprint in preparation.

[28] R. Kögerler and D. Schildknecht, CERN-TH. 3231 (1982).
H. Fritzsch, R. Kögerler and D. Schildknecht, Phys. Lett. **114B**, 157 (1982).

[29] B. Schrempp and F. Schrempp, DESY preprint 84-055 (1984).

[30] D. Denegri (UA1 Collaboration), talk at the 6th Topical Workshop on Proton-Antiproton Physics, Aachen, 1986.

[31] W. Buchmüller, Phys. Lett. **145B**, 151 (1984).

[32] M. Kuroda, D. Schildknecht and K.H. Schwarzer, Nucl. Phys. **B261**, 432 (1985).

[33] C. Korpa and Z. Ryzak, Phys. Rev. **D34**, 2139 (1986).

[34] M. Kuroda and D. Schildknecht, Phys. Lett **121B**, 173 (1983).

[35] U. Baur, D. Schildknecht and K.H. Schwarzer, Max-Planck-Inst. Munich preprint MPI-PAE/PTh 29/85 (1985), to appear in Phys. Rev. D.

[36] U. Baur, M. Lindner and K.H. Schwarzer, preprint in preparation.

[37] D. Dominici, Univ. Florence preprint.

[38] B.W. Lee, C. Quigg and H.B. Thacker, Phys. Rev. **D16**, 1519 (1979).
M.B. Einhorn, Nucl. Phys. **264B**, 75 (1984).
R. Casalbuoni, D. Dominici and R. Gatto, Phys. Lett. **147B**, 419 (1984).

[39] R. Casalbuoni, S. De Curtis, D. Dominici and R. Gatto, Univ. Geneva preprint UGVA-DPT 1986/01- 492 (1986).

[40] L.F. Abbott and E. Farhi, Phys. Lett. **101B**, 69 (1981) and Nucl. Phys. **B189**, 547 (1981).

[41] M. Claudson, E. Farhi and R.L. Jaffe, Phys. Rev. **D34**, 873 (1986), and references therein.
J. Wudka, Phys. Lett. **167B**, 337 (1986).

[42] H. Harari, Phys. Lett. **156B**, 250 (1985) and references therein.

[43] F.M. Renard, Phys. Lett. **166B**, 229 (1986).

[44] B. Schrempp and F. Schrempp, Phys. Lett. **153B**, 101 (1985).

[45] K. Hamacher, internal note to the Working Group.

[46] P. Mättig et al., internal note to the Working Group, preprint in preparation.

[47] F.M. Renard, Phys. Lett. **116B**, 269 (1982).
F. Schrempp, internal note to the Working Group.

**APPENDIX 1**

The unpolarized differential cross-section for Bhabha scattering, including $\gamma$ and Z exchanges, is (Ref. [4])

$$\frac{d\sigma}{d\cos\theta} = (\pi\alpha^2/4s) \cdot [4A_o + A_-(1 - \cos\theta)^2 + A_+(1 + \cos\theta)^2] \qquad (A1.1)$$

where

$$A_o = (\frac{s}{t})^2 \cdot \left| 1 + \frac{g_R g_L}{e^2} \frac{t}{t_z} + \frac{\eta_{RL} \cdot t}{\alpha\Lambda_c^2} \right|^2$$

$$A_- = \left| 1 + \frac{g_R g_L}{e^2} \frac{s}{s_z} + \frac{\eta_{RL} \cdot s}{\alpha\Lambda_c^2} \right|^2$$

$$A_+ = \frac{1}{2} \left| 1 + \frac{s}{t} + \frac{g_R^2}{e^2} \cdot (\frac{s}{s_z} + \frac{s}{t_z}) + \frac{2\eta_{RR} s}{\alpha\Lambda_c^2} \right|^2$$

$$+ \frac{1}{2} \left| 1 + \frac{s}{t} + \frac{g_L^2}{e^2} (\frac{s}{s_z} + \frac{s}{t_z}) + \frac{2\eta_{LL} s}{\alpha\Lambda_c^2} \right|^2$$

with

$$t = -s(1 - \cos\theta)/2; \quad s_z = s - m_z^2 + im_z\Gamma_z,$$

$$t_z = t - m_z^2, \; g_R/e = \tan\theta_w, \; g_L/e = -\cot 2\theta_w$$

Note that contact interactions contribute to both, s-channel and t-channels diagrams. For $e^+e^- \to \mu^+\mu^-$ scattering the differential cross-section is easily obtained from eq. (A1.1) by setting all terms which contain t or $t_z$ to zero and replacing the factor of 2 in front of $\eta_{RR}$ and $\eta_{LL}$ by 1.

The differential cross-section for polarized beams, following the same ansatz for the contact interactions as in the unpolarized case, can be calculated using helicity amplitudes.

Let us define $P_L^{\pm}$ = degree of longitudinal polarization of initial $e^{\pm}$, each oriented along its momentum, and $P_T^{\pm}$ = degree of transverse polarization of initial $e^{\pm}$.

For transverse polarization of the $e^{\pm}$ beams perpendicular to the plane of the ring, $\alpha_{\pm}$ is $\mp\pi/2$. Choosing the z axis to be the electron direction, we find [5] for the differential cross-section:

$$\begin{aligned}
\frac{d\sigma}{d\Omega} = \frac{\alpha^2 s}{16} \cdot \; & |G_{LL}(t) + G_{LL}(s)|^2 \, (1 + P_L^+)(1 - P_L^-) \\
& + |G_{RR}(t) + G_{RR}(s)|^2 \, (1 - P_L^+)(1 + P_L^-) \; ] \cdot (1 + \cos\theta)^2 \\
& + 8 \, |G_{LR}(t)|^2 \, (1 + P_L^+ \, P_L^-) \\
& + 2 \, |G_{LR}(s)|^2 \, (1 - P_L^+ \, P_L^-) \cdot (1 - \cos\theta)^2 \\
& + 2 \, \mathrm{Re} \, [( \, G_{LL}(s) + G_{RR}(s) + G_{LL}(t) + G_{RR}(t) \, ) \, G_{LR}^{*}(s)] \\
& \cdot P_T^+ \, P_T^- \cos(2\phi) \, \sin^2\theta \\
& + 2 \, \mathrm{Im} \, [( \, G_{LL}(s) - G_{RR}(s) + G_{LL}(t) - G_{RR}(t) \, ) \, G_{LR}^{*}(s)] \\
& \cdot P_T^+ \, P_T^- \sin(2\phi) \, \sin^2\theta
\end{aligned} \tag{A1.2}$$

with

$$G_{AB}(x) = \frac{g_A g_B / e^2}{x_Z} + \frac{1}{x} + \frac{1}{\alpha \Lambda_c^2} \, \eta_{AB}$$

$$x_Z = s_Z, t_Z; \quad x = s, t$$

where $g_R$, $g_L$, $s_Z$, $t_Z$, and $\eta_{AB}$ are defined as in eq. (A1.1).

**APPENDIX 2**

In presence of an isoscalar vector boson Y or $Y_L$, the Z mass $M_Z$ and the Y ($Y_L$) mass $M_Y$ are given by

$$\left.\begin{matrix} M_Z^2 \\ M_Y^2 \end{matrix}\right\} = 1/[2(1 - \lambda_W^2 - \lambda_Y^2)] \left\{(1 - \lambda_Y^2)\, m_W^2 + (1 - \lambda_W^2) m_Y^2 \mp \right.$$
$$\left. \mp \sqrt{[(1 - \lambda_Y^2) m_W^2 - (1 - \lambda_W^2) m_Y^2]^2 + 4\, \lambda_W^2 \lambda_Y^2\, m_W^2 m_Y^2} \right\} . \qquad \text{(A2.1)}$$

The vector and axial-vector couplings of the Z [see Eq. (32)] are given by [10]

$$A_Z^{(Y)} = e/b_Z\, [M_Z^2/(M_Z^2 - m_W^2)]\, [(m_Y^2 - m_W^2)/(M_Z^2 - m_Y^2)]\, T_3$$
$$V_Z^{(Y)} = 2\, (e/b_Z)\, (m_Y^2/M_Z^2 - m_Y^2)\, Q - A_Z^{(Y)} \qquad \text{(A2.2)}$$

in the presence of a Y boson, and by

$$A_Z^{(Y_L)} = -\, (e/b_Z)\, [M_Z^2/(M_Z^2 - m_Y^2)]\, Q - A_Z^{(Y)}$$
$$V_Z^{(Y_L)} = -\, (e/b_Z)\, \{1 - [m_Y^2/(M_Z^2 - m_Y^2)]\}\, Q - A_Z^{(Y)} \qquad \text{(A2.3)}$$

in presence of a $Y_L$ boson.

The vector and axial-vector couplings of the corresponding Y and $Y_L$ bosons are given by [10]

$$A_Y = e/b_Y\, [M_Y^2/(M_Y^2 - m_Y^2)]\, [(m_Y^2 - m_W^2)/(M_Y^2 - m_W^2)]\, T_3 ,$$
$$V_Y = 2\, (e/b_Y)\, [m_Y^2/(M_Y^2 - m_Y^2)]\, Q - A_Y , \qquad \text{(A2.4)}$$

and

$$A_{Y_L} = -\, (e/b_Y)\, [M_Y^2/(M_Y^2 - m_Y^2)]\, Q + A_Y ,$$
$$V_{Y_L} = -\, (e/b_Y)\, \{1 - [m_Y^2/(M_Y^2 - m_Y^2)]\}\, Q - A_Y , \qquad \text{(A2.5)}$$

respectively, with

$$b_i^2 = 1 - \lambda_W^2 - \lambda_Y^2 + \lambda_W^2 [m_W^4/(m_W^2 - M_i^2)^2] + \lambda_Y^2 [m_Y^4/(m_Y^2 - M_i^2)^2] , \quad \text{for } i = Z,Y , \qquad \text{(A2.6)}$$

$T_3$ = third component of the global SU(2) isospin, and $Q$ = electromagnetic charge.